A

DISSERTATION REPORT

ON

DESIGN OF OPTICAL LOGIC GATES AND HALF ADDER USING ELECTRO-OPTIC EFFECT IN MACH-ZEHNDER INTERFEROMETER

is submitted as a partial fulfillment of the degree of

MASTER OF TECHNOLOGY

in

WIRELESS AND OPTICAL COMMUNICATON

to the

DEPARTMENT OF ELECTRONICS AND COMMUNICATION ENGINEERING

by

MANISHA PRAJAPAT

(2017PWC5407)

Under the guidance of

Dr. GHANSHYAM SINGH

Electronics & Communication Engineering Department

Malaviya National Institute of Technology, Jaipur

JULY 2019

DEPARTMENT OF ELECTRONICS & COMMUNICATION ENGINEERING
MALAVIYA NATIONAL INSTITUTE OF TECHNOLOGY
JAIPUR (RAJASTHAN) – 302017

<u>Certificate</u>

This is to certify that the dissertation report entitled **Design of Optical logic gates and Half Adder using electro-optic effect in Mach-Zehnder Interferometer** submitted by **Manisha Prajapat (2017PWC5407)**, in the partial fulfilment of the Degree Master of Technology in **Wireless and Optical Communication** of Malaviya National Institute of Technology, is the work completed by her under our supervision, and approved for submission during academic session 2018-2019.

Dr. Ghanshyam Singh

(Project Supervisor)

Professor

Date: Dept. of ECE

Place: MNIT Jaipur, India

<u>Declaration</u>

I, **Manisha Prajapat,** declare that this Dissertation titled as "**Design of Optical logic gates and Half Adder using electro-optic effect in Mach-Zehnder Interferometer**" and the work presented in it is my own and that, to the best of my knowledge and belief.

I confirm that the major portion of the report except the refereed works, contains no material previously published nor present a material which to be substantial extent has been accepted or the award of any other degree by university or other institute of higher learning. Wherever I used data (Theories, results) from other sources, credit has been made to that source by citing them (to the best of my knowledge). Due care has been taken in writing this thesis, errors and omissions are regretted.

Date :   **Manisha Prajapat**

Place :   ID : 2017PWC5407

Acknowledgment

I would like to thank all peoples who have helped me in this project, directly or indirectly.

I take immense pleasure in thanking of gratitude to my project supervisor **Dr. Ghanshyam Singh***, Professor, Malaviya National Institute of Technology (MNIT) Jaipur for being a source of inspiration and for timely guidance during the project. The supervision and support that he gave truly helped in the progression of my thesis. I am highly obliged to him for his valuable advices and moral support during research period.*

I express my sincere gratitude to **Prof. D. Boolchandani** *(Head of Department) for his support and guidance in this research work. Many thanks to committee members Dr. Vijay Janyani (Professor), Dr. Ritu Sharma (Associate Professor), Dr. M. Ravi Kumar (Assistant Professor), and Dr. Ashish Kumar Ghunawat (Assistant Professor) for their valuable comments and guidance in research exploration, without this guidance it was not possible to achieve these good results in this research work. I would like to thank Ankur Saharia (Phd Scholar) for their valuable suggestions and discussion, which I had with them about this research work. I would like to thank Mr. Vijay Singh and Mr. Deepak for allowing me in laboratories over time.*

I am also very thankful to my friends for their valuable suggestions and discussion, which I had with them about this research work. They also help me in designing work of my project.

I would also like to thank Ministry of HRD, Government of India for its support to me to pursue my Masters in Wireless and Optical Communication Engineering from Malaviya National Institute of Technology, Jaipur. This support provided me library, laboratory and other related infrastructure.

Finally, my greatest and special gratitude goes to my family for their love and support.

Manisha Prajapat

Abstract

In this work the effective applicability of electro-optic effect for the implementation of all logic gates in optical domain and Half Adder using Mach-Zehnder Interferometers (MZI) has been demonstrated. Performance enhancement using electro-optic switch implemented using MZIs based on Titanium diffused Lithium Niobate (Ti:LiNbO$_3$) functioning as waveguide medium at 1.33 µm wavelength is detailed in the work. The designs implemented consist of one MZI for NOT gate, two MZIs for AND gate, three MZIs for OR gate, two MZIs for NOR gate, three MZIs for NAND gate, two MZIs for XOR gate, two MZIs for XNOR gate and three MZIs for half adder which are giving optimized operation in terms of low insertion losses, high extinction ratio and low switching voltage. Further the titanium strip thickness was varied and analysis of the device performance has been done. Mathematical description of the device operation is also included and the obtained results of MATLAB simulations and beam propagation method applied were compared and verified.

The primary goal of developing the methods of optical digital computing is to significantly improve fundamental and complicated digital equipment. Optical digital computing methods offer the best choice for high-speed processing of data. It can allow huge numbers of functions for signal processing like switching, addressing, encoding, and complicated digital computations. The EO effect is also very extensively investigated for the optical logic gates realization. For simplifying the system, the optical switching can be made using the EO effect in MZI. For optical signal processing and optical fiber communication, a Ti diffused lithium niobate waveguide is beneficial. The optical switching phenomenon has been researched in LiNbO3-based MZIs and its efficiency has been demonstrated in implementing multiple logic gates in optical domain, combinational circuits and routers. By using this phenomenon all logic gates in optical domain and combinational circuits are implemented using beam propagation method and results of these designs are verified using equations of mach-zehnder interferometer in MATLAB simulation.

List of Abbreviation

2D	-	Two Dimensions
3D	-	Three Dimensions
ADI	-	Alternate Direction Implicit
BPM	-	Beam Propagation Method
CAD	-	Computer Added Design
CFM	-	Correlation Function Method
EO	-	Electro Optic
ER	-	Extinction Ratio
IL	-	Insertion Loss
$LiNbO_3$	-	Lithium Niobate
MZI	-	Mach Zehnder Interferometer
OEO	-	Optical Electrical Optical Conversion
RI	-	Refractive Index
TBC	-	Transparent Boundary Condition
TDM	-	Time Domain Multiplexer
TE	-	Transverse Electrical
Ti	-	Titanium
$Ti:LiNbO_3$	-	Titanium diffused Lithium Niobate
TM	-	Transverse Magnetic
TMM	-	Transfer Matrix Method
SOA	-	Semiconductor Optical Amplifier
WDM	-	Wavelength Division Multiplexer

List of Symbols

µm	-	Micrometer
eV	-	Electron Volt
dB	-	Decibel
D_H	-	Lateral Diffusion Length
D_V	-	Diffusion Length Depth
E	-	Electric Field
G	-	Gram
K	-	Kelvin
L	-	Length of Electrode Region
mm	-	Millimeter
mw	-	Milliwatt
N	-	Refractive Index
nm	-	Nanometer
P_{in}	-	Power at output
P_{off}	-	Power at output for output low or 0
P_{on}	-	Power at output for output high or 1
P_{out}	-	Power at output
R	-	Electro-optic coefficient
V	-	Voltage
V_π	-	Voltage at $\Delta\varphi = \pi$
Δn	-	Effective Refractive Index
$\Delta\varphi$	-	Phase change
Λ	-	Wavelength
P_{out1}	-	Power at out port 1
P_{out2}	-	Power at out port 2

Table of Contents

List of Figures

xi

List of Tables

CHAPTER 1: INTRODUCTION

1.1 Introduction

Today there has been a rapid increase in high bandwidth demand to achieve the electronic devices' speed limit. Signal processing of all optical devices' overall aim is still on the horizon. The ideal design of high-bit-rate logic gates in optical domain is now coming out of the laboratories. In this sector, the researchers are moving forward to make this possible. However, logic gates in digital domain have complex and bulky electro-optic transformation for signal processing in optical domain [1]. Electro-optic MZI has been widely used in optical systems recently due to high speed operation requirements. They find wide applicability due to their inherent advantages of reliability and high speed switching capabilities which makes them competent candidates in next generation optical networks. In the field of optoelectronics, high-speed communication has been achieved by virtue of low complexity offered by these devices where optimization perform a major task in the fast processing of optical data [2]. To make the dream come true, optical gates are the fundamental necessity. Gates are the main components for performing all-optical tasks. Therefore, to realize digital gates on the same platform into all-optical logic gates, several fundamental designs need to be developed [3].

Due to increased bandwidth demand, the scale of electronic devices to higher transmission rates is particularly challenging owing to their dissipation of power and use of energy [4-5]. Changing the optical packet is a pleasant replacement for boosting the forwarding speed of the router. An important segment of any router is a memory unit needed to store a packet's header intelligence shortly [6].

For high-speed telecommunication systems, optical logic gates require significant elements as they have to achieve various functionalities in optical signal processing like switching, regeneration, addressing, multiplexing/demultiplexing, decision making, computation, coding/decoding and so on [7]. MZI switch is designed using titanium diffused lithium niobate because of which high speed of operation above the 40 Gb/s at long haul optical transmission system, large capacity, TE field in the direction of propagation, and zero residual birefringence, less complexity and high EO coefficient for less switching time can be attained [8-9]. Different types of materials and their configurations have been examined in this work to get the desired all-optical switches. For this purpose, the materials should possess high non-linearity

characteristics, low operating voltage to ensure quick response times and low switching losses in switching operation. Further, thermo-optic effect and electro-optic effect can also be employed [10].

Due to its unique characteristics of large bandwidth, low distortion of signal distribution, spatial coherence and high spectral, robustness of cosmic radiation's robustness, and RF interference which is free, signal processing of optical digital has drawn extensive study interest in past years. Although different writers have shown their keen interest in designing the digital logic gates using different optical processing methods in the past, while designing of universal gates is the main problem in the processing of optical signals. NAND and NOR gates are called universal because with the support of these universal logic gates, all other logic operations can be performed [11-13]. A novel method is suggested to use the EO effect in MZI to create universal gates. Because of the electro-optic (EO) impact, the fundamental switching element in LiNbO$_3$-based MZI is described. The LiNbO$_3$ based MZI is distinguished by small size, thermal stability, reconfigurability, integration potential, low latency, and low power consumption appealing characteristics [14]. As a result, many researchers showed a keen interest in designing various combinational and sequential circuits using EO effect in MZIs. Universal logic gates implementation using LiNbO$_3$-based MZI's electro-optic effect was illustrated in which writers developed that by inverting an AND operation output, the NAND gate is deployed and similarly, by inverting the OR operation output, the NOR gate is intended [15].

1.2 Objectives

The primary goal of developing the methods of optical digital computing is to significantly improve fundamental and complicated digital equipment. Optical digital computing methods offer the best choice for high-speed processing of data. It can allow huge numbers of functions for signal processing like switching, addressing, encoding, and complicated digital computations [16-17]. Many scholars have demonstrated the various processes for implementing the various combinational and sequential logic circuits. Using multiple optical signal processing methods, the fundamental combination logic gates such as AND Gate, OR Gate, and NOT logic gates are applied [18]. The EO effect is also very extensively investigated for the optical logic gates' realization. For simplifying the system, the optical switching can be made using the EO effect in MZI [19]. To introduce the optical switches, the

electro-optic effect in MZI was used efficiently. Effectively study the switching phenomena in optical, the EO effect in MZI and implementation of optical combinational circuits is commonly investigated [20]. Major role of proper switching technology in determining any network's workable design and can effectively enhance precision, flexibility, scalability and speed [21]. In electronic switching optoelectronic conversion takes place whereas in optical switching optoelectronic conversion is not occurring. Optical switch's speed and sensitivity must exactly match with photonic networks of new generation, where light directly regulates the switches in its route and carries data and routing information, but also. The lithium niobate electro-optic coefficient is well adapted for quick optical communication systems modulation and switching [21]. For optical signal processing and optical fiber communication, a Ti diffused lithium niobate waveguide is beneficial. The optical switching phenomenon has been researched in LiNbO3-based MZIs and its efficiency has been demonstrated in implementing multiple logic gates in optical domain, combinational circuits and routers [22]. By using this phenomenon all logic gates in optical domain and combinational circuits are implemented using beam propagation method and results of these designs are verified using equations of mach-zehnder interferometer in MATLAB simulation.

1.3 Thesis Organization

This thesis is organized in 7 chapters containing this introduction chapter. Following the introduction chapter, chapter 2 describe the literature survey of proposed work on optical logic gates and half adder using electro-optic effect in MZI.

In chapter 3, we have describe the basic idea of the electro optic effect, properties of Lithium Niobate material and Titanium diffusion in Lithium Niobate, MZI switch behaviour and its mathematical equations are explained in detailed.

In chapter 4, we have discuss about the block diagram of all logic gates like NOT, AND, OR, NOR, NAND, XOR, XNOR gates and half adder, and their mathematical equations and by these equations MATLAB simulation graph is explained.

In chapter 5, simulator tool OPTI-BPM is discussed. How we can design a device through it and how any device is simulated in this simulator all steps are explained in this chapter. Design process of a basic MZI switch is also explained. Taking this design as a reference design, I have designed rest of all new designs.

In chapter 6, all designs, their optical field and obtained their graph of insertion loss and extinction ratio by varying Ti strip thickness are done. By the graph we obtained maximum value of extinction ratio and minimum value of insertion loss for all designs.

Finally in chapter 7, conclusion of whole project and future work which can be done after this work is explained.

CHAPTER 2: LITERATURE SURVEY

Ganguly, P. et. al. (1996) "Simulation of refractive index profiles for titanium in diffused lithium niobate channel waveguides" [6]. In this paper, Ti diffused waveguide on Y–cut and Z-cut lithium niobate substrate and observe refractive index for single and coupled waveguides using BPM.

Singh G. et. al. (2010) "Ti in diffused lithium niobate (Ti: LiNbO$_3$) Mach-Zehnder interferometer all optical switches: a review" [8]. In this paper, detailed about switching characteristics of MZI switch based on EO effect using Ti: LiNbO3 in waveguides. Losses are compare of this design with SOA-MZI and observe the extinction ratio an insertion loss.

Singh G. et. al. (2011) "Modeling of a 2× 2 electro-optic Mach-Zehnder Interferometer optical switch with s-bend arms." [3]. In this paper, MZI switch with s-bend interferometric arms is designed using Ti: LiNbO3. And observe the cross talk, extinction ration and switch losses.

Singh Ghanshyam et. al. (2012) "Modeling of a high performance Mach--Zehnder interferometer all optical switch." [2]. In this paper MZI switch is designed using Ti: LiNbO3. Optimize and modeled Ti diffusion process and observe the impact of Ti strip thickness on cross talk, transition losses and first 3 dB coupler's power imbalance.

Mohammed, Nazmi A. et. al. (2012) "Performance Evaluation and Enhancement of 2× 2 Ti: LiNbO3 Mach Zehnder Interferometer Switch at 1.3 µm and 1.55 µm." [16]. In this paper implement EO 2x2 switching device using Ti:LiNbO$_3$ as waveguide at 1.33 µm and 1.55 µm. Observe IL and ER for both wavelength. Capability and reliability of this switch is very high.

Kumar, et. al. (2013) "Implementation of optical switches using Mach–Zehnder interferometer." [4]. In this paper, observe effect of voltage which is varying of every electrode of the MZI structure. The results of this design are useful to design optical logic gate and the single router in dense wavelength division multiplexing.

Kumar, et. al. (2015) "Design of D flip-flop and T flip-flop using Mach–Zehnder interferometers for high-speed communication." [7]. In this paper, speed of communication is low by using electrical component while using optical component

speed of communication is high. Different combinational circuits are designed using EO effect based MZI and results are obtained by BPM and MATLAB simulations.

Kumar, et. al. (2015) "Proposed new approach to the design of universal logic gates using the electro-optic effect in Mach–Zehnder interferometers." [11]. In this paper, universal logic gates (NAND and NOR) are designed based on EO effect using Ti:LiNbO$_3$ in MZI on BPM and results are verified by the MATLAB simulation. Observe the speed, latency and power consumption etc. influencing parameters.

Khatun, et. al. (2015) "Optimization of 2× 2 MZI electro-optic switch and its application as logic gate." [19]. In this paper, EO-MZI is designed at 1.55 µm for high speed of operation. Observe high ER, low IL and low switching voltage. Capability and reliability of this switch is very high.

Kumar Harsh, et. al. (2017) "Gray to binary code converter using Ti-in diffused lithium niobate based Mach-Zehnder interferometer." [1]. In this paper describe that using XOR logic, 3 bit gray to binary code convertor designed using Ti:LiNbbO$_3$ in MZI. At the output optical signal is obtained in form of binary. This device provides high speed of switching, minimum losses and high extinction ratio.

MS Windows NT mzi switch optiwave, Accessed: 2019-06-03 [24]. This link provides the designing steps of MZI switch using Opti-BPM software and learn about this beam propagation method platform for designing of the proposed device.

CHAPTER 3: ELECTRO-OPTIC EFFECT IN MACH-ZEHNDER INTERFEROMETER

3.1 Introduction

One of the most significant mediums to impose data on or modulate a light wave carrier is the EO effect. Electro-optic devices are created to be used for modulation or switching or so many purposes in optical communications. Example devices include phase and amplitude modulators. The electro-optic effect enables frequency modulation to be much greater than other techniques, such as mechanical shutters, moving mirrors or acousto-optic equipment, owing to quicker response time.

The fundamental concept behind electro-optic systems is to alter in a controlled manner the material's optical properties with an applied electric field. An optical signal's shift in optical properties refers to change in phase, amplitude, frequency, polarization, or position as it propagates through the device. According to change in properties we differentiate the electro-optic effect [8].

3.2 Electro-Optic Effect

Some materials have the property that if an optical signal passes through it, its properties change according to applied external force. Reasons to change these properties are change in positions, orientations, or shapes of the molecules originating from the material by applying any external forces eg. Voltage, temperature, acoustic waves etc. The shift in the refractive index arising from the implementation of an electrical dc or low frequency field known as the electro-optic effect [8].

3.3 Lithium Niobate- A crystal for optical processing

In linear and non-linear applications different kind of devices can be included like mobile device, optical modulators and sensors based on piezo-elecric effect all these are based Lithium Niobate crystal material. It is a compound material made of niobium, lithium, and oxygen, Lithium Niobate has a trigonal geometry class of R3c and 3m point group framework without anti symmetry and show properties of Ferroelectricity, Pockel's impact, piezoelectric impact, photo elasticity and nonlinear optical polarizability. It is a hard no soluble in water having negative uniaxial birefringence dependent on the stoichiometry and temperature of the crystal. It can be operate under the range of 350 and 5200 nm wavelength. Single crystal of LN wafers

grown using the Czochralski process after then wafer is cut into different cuts eg. Z-cut, X-cut, Y-cut

Lithium Niobate ($LiNbO_3$) is a colourless. It is insoluble with water. $LiNbO_3$ is a ferroelectric material. In integrated optics developers use its electro-optical characteristics, acousto-optical characteristics and non-linear optical characteristics and proved to be optical waveguides manufacture with great material. For communication technology high bandwidth property makes appropriate intrinsic modulation.

Specification of lithium Niobate are described as that chemical formula of lithium Niobate is $LiNbO_3$, crystal glass is trigonal with 3m, lithium Niobate is non-soluble in water and colourless, molecular weight is 147.9 g/mol, density is 4.644 g/cm^3, transmittance range is 350-5500 nm, melting point is 1530 K, curie temperature is 1415 K, thermal conductivity is 5.6 W/(m K) at 300 K, and bandgap is 4 eV.

For multiple technical innovations, it's piezoelectric and photo elastic characteristics were used. By virtue of its large EO coefficient, resistance of optical damage and minimum losses, lithium niobate was used to manufacture embedded waveguides. For wavelength-tunable polarization converters implementation Strain-optic impacts are used. To design low-loss switches, $LiNbO_3$ material has been used widely, but the main problem is their polarization dependence. For high and low velocity schemes, the selection of Lithium Niobate based switches is proven to be the best. The requirements of modulation in digital fiber optic TDM and WDM schemes have been effectively resolved by $LiNbO_3$ devices in latest years [8].

3.4 Ti-diffused Lithium Niobate

Waveguides which made of lithium niobate material can be manufactured using either in-diffusion of titanium or annealed proton exchange procedures to design switches and modulators. The entire $LiNbO_3$ is subjected to the manufacture of planner waveguides while, with these procedures, the photolithography method is used to define masks for chosen areas on it. In some cases, to control optical damage, Mg oxide is doped with LiNbO3. The lithium niobate waveguides exchanged for protons are simple to manufacture and can function at low temperatures. For multiple communication, sensor systems and signal processing, Ti diffused lithium niobate waveguides are helpful. Ti doping in lithium niobate crystal increases refraction

indexes, allowing both TE and TM modes to propagate along the wave guides, which fulfils the necessary optical signal processing requirements [22].

3.5 MZI Switch

Mach–Zehnder interferometer (MZI)-based structures are among the numerous techniques available to transform a modulation of phase into a modulation of intensity. These designs are widely used by electro-optic (EO) or thermo-optic (TO) impacts to create a various applications like optical modulators, splitters, switches, etc. The symmetric MZI structure was proposed to design high speed switches for lower bandwidth operation using the EO effects. Lithium niobate (LN) is an appropriate material for MZI structure based switches because of its large EO-coefficients, but a latest material potassium niobate (KN) has recently been discovered that can substitute lithium niobate. These systems have stable performance parameters, even for inputs with a broad range of concentrations of optical power.

Under the influence of an electric field MZI switches produce the refractive index in optical medium, due to this bending of light occur through the medium, this phenomenon is known as phase modulation. By optimized different design parameters like diffusion parameter, dimension of the waveguide, applied field etc., increase the performance of switch [9].

3.6 Mathematical Equations

The refractive index of the light propagating through the arms of the interferometer faces a change on application of an electrical voltage. This variation in refractive index introduces phase shifts in the lights propagating through them which lead to a resultant output port switching. This transduction phenomenon is widely named as electro-optic effect where the light at the output port switches with application of an input bias [19]. The schematic layout of 2x2 MZI switch used in simulation analysis is shown in fig. 3.1
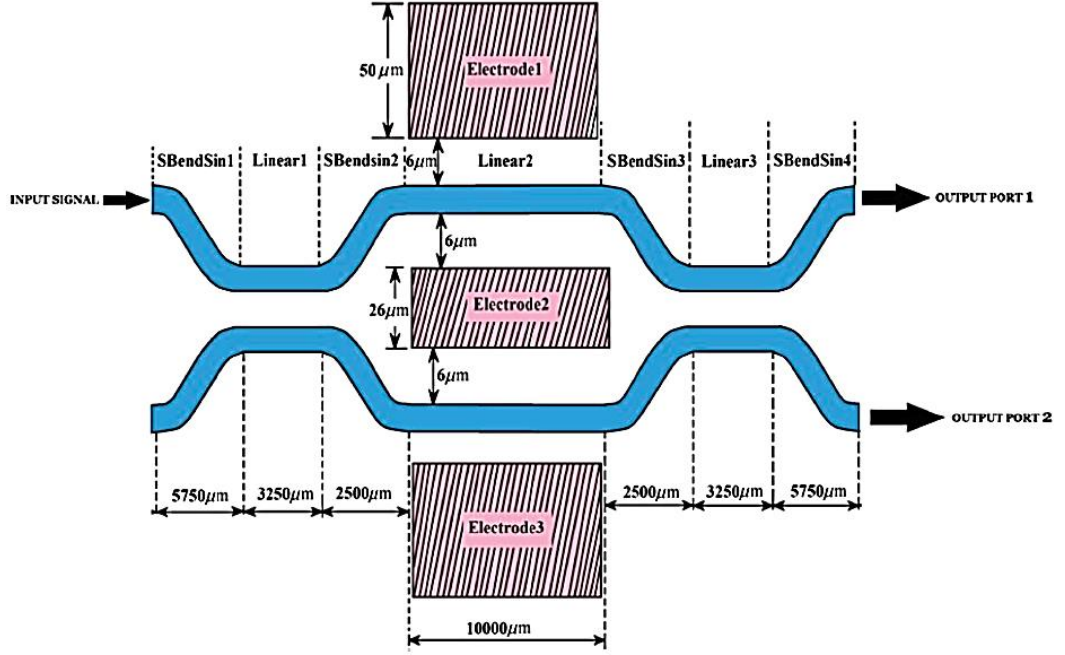
Figure 3.1: Structure of MZI [4]

Following equation can be used to find out the corresponding phase change [19].

$$\Delta\varphi = \frac{2\pi}{\lambda}(\Delta n)L \qquad (3.1)$$

Where, L is substantial length of interferometer arm

Δn is the change in refractive index due to applied voltage that is represented by [19]

$$\Delta n = \left(\frac{n^3}{2}\right)rE \qquad (3.2)$$

r is electro-optic coefficient. For LiNbO3, r = 3.66× 10^{-10} m/V.

And $\Delta\varphi$ is shown below [19],

$$\Delta\varphi = \frac{2\pi}{\lambda}\left[\left(\frac{n^3}{2}\right)rE\right]L \qquad (3.3)$$

Let the distance between the two electrodes in figure 1 is d and the voltage difference between them to be V, then find E approximately equal to V/d. Then eq. (3.3) can deduce to eq. (3.4) [19].

$$\Delta\varphi = \frac{2\pi}{\lambda}\left[\left(\frac{n^3}{2}\right)\frac{V}{d}r\right]L \qquad (3.4)$$

If $\Delta\varphi$ = zero, then it shows no voltage is applied. And when V is applied, then $\Delta\varphi = \pi$. At this point, voltage is known as V_π and is represented by eq. (3.5) [19].

$$V_\pi = \frac{\lambda}{n^3}\frac{1}{r}\frac{d}{L} \qquad (3.5)$$

Now output ports normalized powers are given by eq. (3.6) [19].

$$P_{out1} = \sin^2\left(\frac{\Delta\varphi}{2}\right)$$

$$P_{out2} = \cos^2\left(\frac{\Delta\varphi}{2}\right) \qquad (3.6)$$

The device performance can be modelled by the IL and ER involved, where IL is the ratio of output power with respect to the input given by equation (3.7) [19].

$$IL(dB) = 10\log_{10}\left(\frac{P_{out}}{P_{in}}\right) \qquad (3.7)$$

Whereas the ratio of circuit ON state power to OFF state output power gives the ER and is given by eq. (3.8) [19].

$$ER(dB) = 10\log_{10}\left(\frac{P_{on}}{P_{off}}\right) \qquad (3.8)$$

CHAPTER 4: MATLAB GRAPH OF ALL LOGIC GATES AND HALF ADDER

4.1 NOT GATE

Figure 4.1 depicts the layout used to structure the proposed NOT Gate. NOT gate inverts the applying input that is when logic 0 is applied at input then logic 1 is received at output and if logic 1 is applied at input then logic 0 I obtained at output.
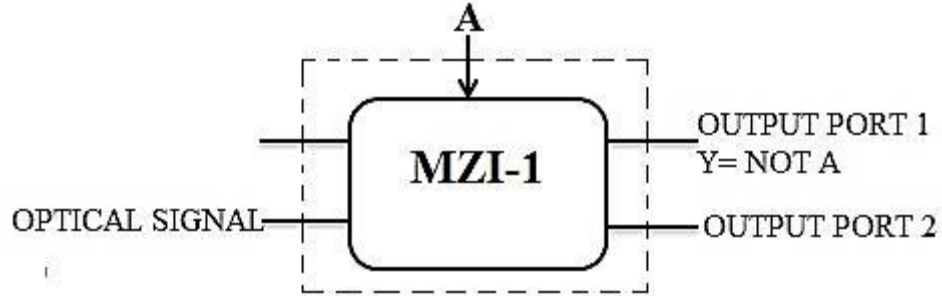

Figure 4.1: Block diagram of NOT Gate

Mathematical equation for normalized power of MZI single staged circuit can be effectively used for normalized power evaluation at the output port of MZI-1 In this work as shown in figure output ports 1 (Fig.4.1) has been used for evaluation. The output power at both the output ports can be evaluated utilizing following equations:

$$m_0 = \left|\frac{\text{OUT2}_{\text{MZI}_1}}{\text{E}_{\text{in}}}\right|^2 = \cos^2\left(\frac{\Delta\varphi_{\text{MZI1}}}{2}\right) \tag{4.1}$$

Eq. (4.1) is solved using the assumption given below,

$$\Delta\varphi_{\text{MZI1}} = \frac{\pi}{V_\pi}A \tag{4.2}$$

Signal A is controlling MZI-1 at second electrode of MZI-1, logic 0 is represented by 0.00V and logic 1 is represented by 6.75V. Hence following expressions for output of proposed NOT Gate can be obtained as:

$$\text{Output port 1 (NOT Gate)} = \left|\frac{\text{OUT1}_{\text{MZI2}}}{\text{E}_{\text{in}}}\right|^2 = m_0 = \cos^2\left(\frac{\Delta\varphi_{\text{MZI1}}}{2}\right) \tag{4.3}$$

Implementation of NOT Gate using MATLAB

To implement the NOT gate single MZI was used, as represented in Fig. 4.1. At the input of MZI-1 the optical signal is applied and output port 1 is taken as output of NOT gate shown in the figure. Fig. 4.2 shows the results of MATLAB analysis of the implemented NOT gate. The first row in Fig. 4.2 represents the input control signals A

used in the simulation. The second row denotes the output obtained which is a NOT operation.
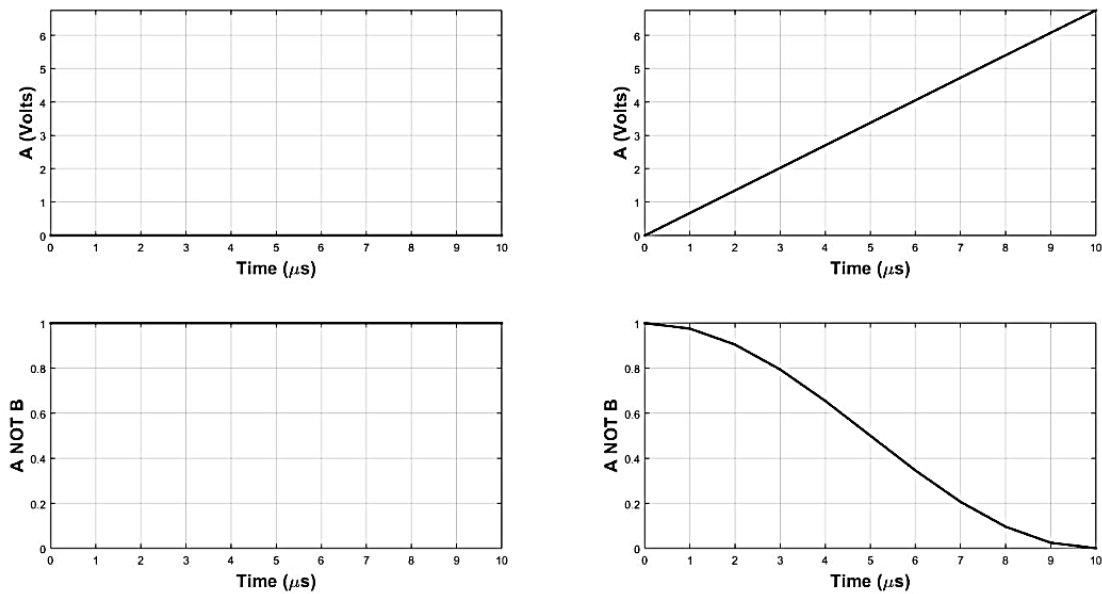

Figure 4.2: MATLAB Simulation results of implemented NOT Gate using MZI's

4.2 AND GATE

Figure 4.3 depicts the layout used to structure the proposed AND Gate. AND gate gives the output logic 1 when it's both inputs are at logic 1, if any input is logic 0 the output will be logic 0.

Figure 4.3: Block diagram of AND Gate

Mathematical equation for normalized power of MZI single staged circuit can be effectively used for normalized power evaluation at the output port of MZI-2. In this work as shown in figure output ports 1 (Fig.4.3) has been used for evaluation. The output power at the output port can be evaluated utilizing following equations:

$$m_3 = \left| \frac{\text{OUT1}_{\text{MZI2}}}{\text{E}_{\text{in}}} \right|^2 = \sin^2\left(\frac{\Delta\varphi_{\text{MZI1}}}{2}\right) \sin^2\left(\frac{\Delta\varphi_{\text{MZI2}}}{2}\right) \tag{4.4}$$

Eqs. (3.4) is solved using the assumptions given below,

$$\left. \begin{aligned} \Delta\varphi_{MZI_1} &= \frac{\pi}{V_\pi}A \\[2mm] \Delta\varphi_{MZI2_2} &= \frac{\pi}{V_\pi}B \end{aligned} \right\} \tag{4.5}$$

Signal A is controlling MZI-1 and Signal B is controlling MZI-2. At second electrode of each MZI, logic 0 is represented by 0.00V and logic 1 is represented by 6.75V. Hence following expressions for output of the proposed AND gate can be obtained as:

Output port 1 (AND logic) $= \left|\dfrac{OUT1_{MZI2}}{E_{in}}\right|^2 = m_3 = \sin^2\left(\dfrac{\Delta\varphi_{MZI1}}{2}\right)\sin^2\left(\dfrac{\Delta\varphi_{MZI2}}{2}\right)$ (4.6)

Implementation of AND Gate using MATLAB

To implement the AND gate two MZI's were used, as represented in Fig. 4.3. At the input of MZI-1 the optical signal is applied and its one of the output port (bar port) is connected to the first input port of MZI-2 and cross port in not connected further. The output port 1 of MZI-2 is taken as output of AND gate shown in the figure. Fig. 4.4 shows the results of MATLAB analysis of the implemented AND gate. The first and second rows in Fig. 4.4 represent the input control signals A and B respectively used in the simulation. The third row denotes the outputs obtained which is the AND operations.

Figure 4.4: MATLAB Simulation results of implemented AND Gate using MZI's

4.3 OR GATE

Figure 4.5 depicts the layout used to structure the proposed OR Gate. OR gate gives output logic 0 when it's both inputs are logic 0, if any of the input is logic 1 then output will be logic 1.
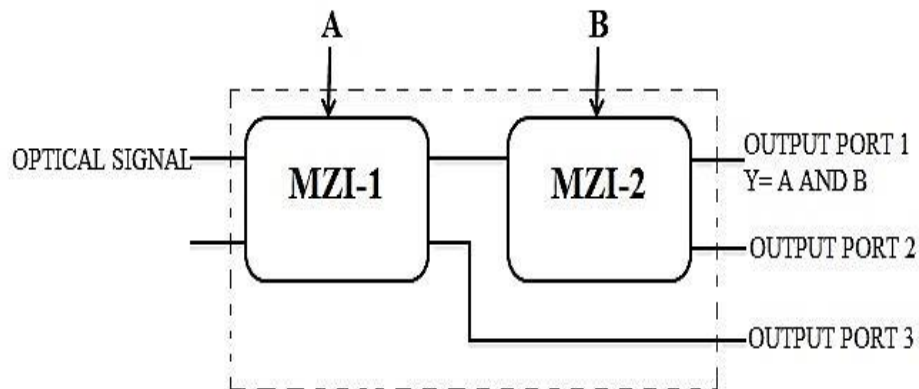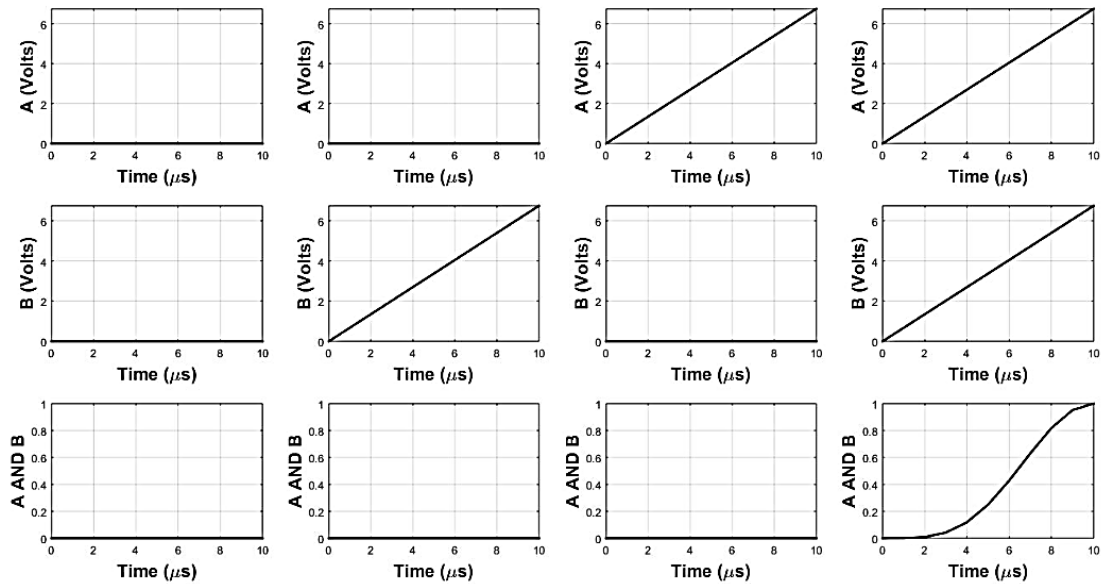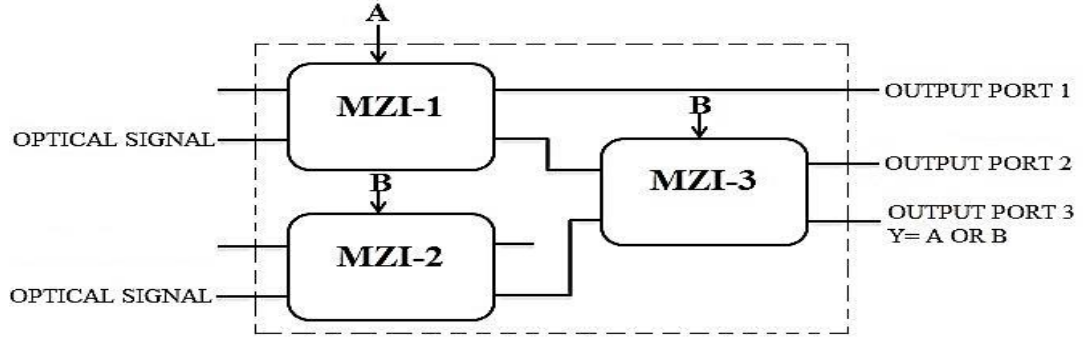

Figure 4.5: Block diagram of OR Gate

Mathematical equation for normalized power of MZI single staged circuit can be effectively used for normalized power evaluation at the output port of MZI-3. In this work as shown in figure output ports 3 (Fig.4.5) has been used for evaluation. The output power at the output port can be evaluated utilizing following equations:

$$m_1 = \left|\frac{OUT1_{MZI3}}{E_{in}}\right|^2 = \cos^2\left(\frac{\Delta\varphi_{MZI1}}{2}\right)\sin^2\left(\frac{\Delta\varphi_{MZI2}}{2}\right)\sin^2\left(\frac{\Delta\varphi_{MZI3}}{2}\right) \tag{4.7}$$

$$m_2 = \left|\frac{OUT1_{MZI3}}{E_{in}}\right|^2 = \sin^2\left(\frac{\Delta\varphi_{MZI1}}{2}\right)\cos^2\left(\frac{\Delta\varphi_{MZI2}}{2}\right)\cos^2\left(\frac{\Delta\varphi_{MZI3}}{2}\right) \tag{4.8}$$

$$m_3 = \left|\frac{OUT1_{MZI3}}{E_{in}}\right|^2 = \sin^2\left(\frac{\Delta\varphi_{MZI1}}{2}\right)\sin^2\left(\frac{\Delta\varphi_{MZI2}}{2}\right)\sin^2\left(\frac{\Delta\varphi_{MZI3}}{2}\right) \tag{4.9}$$

Eqs. (3.7)- (3.9) are solved using the assumptions given below,

$$\left.\begin{array}{l} \Delta\varphi_{MZI_1} = \frac{\pi}{V_\pi}A \\[2mm] \Delta\varphi_{MZI_2} = \frac{\pi}{V_\pi}B \\[2mm] \Delta\varphi_{MZI_3} = \frac{\pi}{V_\pi}B \end{array}\right\} \tag{4.10}$$

Signal A is controlling MZI-1 and Signal B is controlling MZI-2 and MZI-3. At second electrode of each MZI, logic 0 is represented by 0.00V and logic 1 is represented by 6.75V. Hence following expressions for output of the proposed AND gate can be obtained as:

Output port 3 (OR logic) $= \left| \frac{OUT1_{MZI2}}{E_{in}} \right|^2 = m_1 + m_2 + m_3$

$$= \cos^2 \left(\frac{\Delta \varphi_{MZI1}}{2} \right) \sin^2 \left(\frac{\Delta \varphi_{MZI2}}{2} \right) \sin^2 \left(\frac{\Delta \varphi_{MZI3}}{2} \right)$$

$$+ \sin^2 \left(\frac{\Delta \varphi_{MZI_1}}{2} \right) \cos^2 \left(\frac{\Delta \varphi_{MZI_2}}{2} \right) \cos^2 \left(\frac{\Delta \varphi_{MZI_3}}{2} \right)$$

$$+ \sin^2 \left(\frac{\Delta \varphi_{MZI1}}{2} \right) \sin^2 \left(\frac{\Delta \varphi_{MZI2}}{2} \right) \sin^2 \left(\frac{\Delta \varphi_{MZI3}}{2} \right) \tag{4.11}$$

Implementation of OR Gate using MATLAB

To implement the OR gate three MZI's were used, as represented in Fig. 4.5. At the input of MZI-1 and MZI-2 the optical signal is applied and one of the output port, bar port of MZI-1 is connected to the first input port of MZI-3 and cross port in not connected further. The bar port of MZI-2 is connected to the second input port of MZI-3. The output port 2 of MZI-3 is taken as output of OR gate shown in the figure. Fig. 4.6 shows the results of MATLAB analysis of the implemented OR gate. The first and second rows in Fig. 4.6 represent the input control signals A and B respectively used in the simulation. The third row denotes the outputs obtained which is the OR operations.
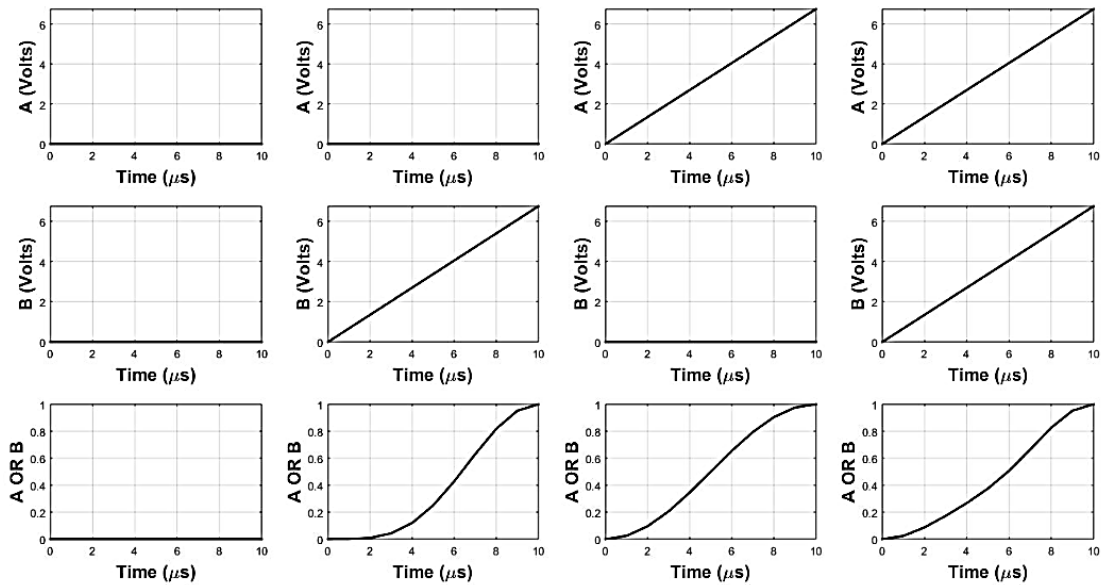

Figure 4.6: MATLAB Simulation results of implemented OR Gate using MZI's

4.4 NOR GATE

Figure 4.7 depicts the layout used to structure the proposed NOR Gate. NOR gate gives output logic 1 when it's both inputs are logic 0, if any of the input is logic 1 then output will be logic 0.
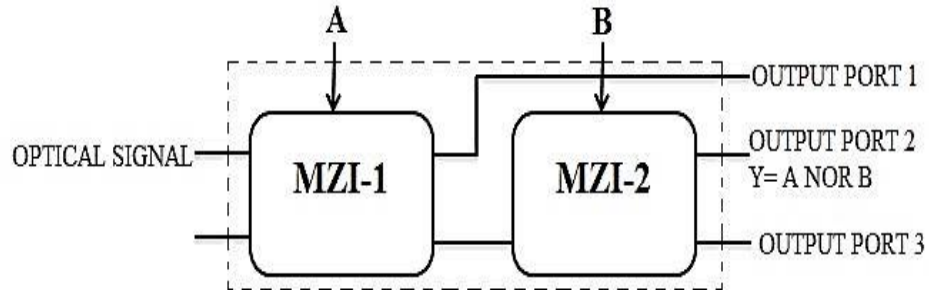

Figure 4.7: Block diagram of NOR Gate

Mathematical equation for normalized power of MZI single staged circuit can be effectively used for normalized power evaluation at the output port of MZI-2. In this work as shown in figure output ports 2 (Fig.4.7) has been used for evaluation. The output power at the output port can be evaluated utilizing following equations [11]:

$$m_0 = \left|\frac{OUT1_{MZI2}}{E_{in}}\right|^2 = cos^2\left(\frac{\Delta\varphi_{MZI1}}{2}\right)cos^2\left(\frac{\Delta\varphi_{MZI2}}{2}\right) \qquad (4.12)$$

Eqs. (4.12) is solved using the assumptions given below [11],

$$\left.\begin{array}{l} \Delta\varphi_{MZI_1} = \dfrac{\pi}{V_\pi}A \\[3mm] \Delta\varphi_{MZI_2} = \dfrac{\pi}{V_\pi}B \end{array}\right\} \qquad (4.13)$$

Signal A is controlling MZI-1 and Signal B is controlling MZI-2. At second electrode of each MZI, logic 0 is represented by 0.00V and logic 1 is represented by 6.75V. Hence following expressions for output of the proposed AND gate can be obtained as [11]:

Output port 1 (NOR logic) = $\left|\dfrac{OUT1_{MZI2}}{E_{in}}\right|^2 = m_0 = cos^2\left(\dfrac{\Delta\varphi_{MZI1}}{2}\right)cos^2\left(\dfrac{\Delta\varphi_{MZI2}}{2}\right)$ (4.14)

Implementation of NOR Gate using MATLAB

To implement the NOR gate two MZI's were used, as represented in Fig.4.7. At the input of MZI-1 the optical signal is applied and its one of the output port (cross port) is connected to the second input port of MZI-2 and bar port in not connected further. The output port 2 of MZI-2 is taken as output of NOR gate shown in the figure.

Fig.4.8 shows the results of MATLAB analysis of the implemented NOR gate. The first and second rows in Fig.4.8 represent the input control signals A and B respectively used in the simulation. The third row denotes the outputs obtained which is the NOR operations.
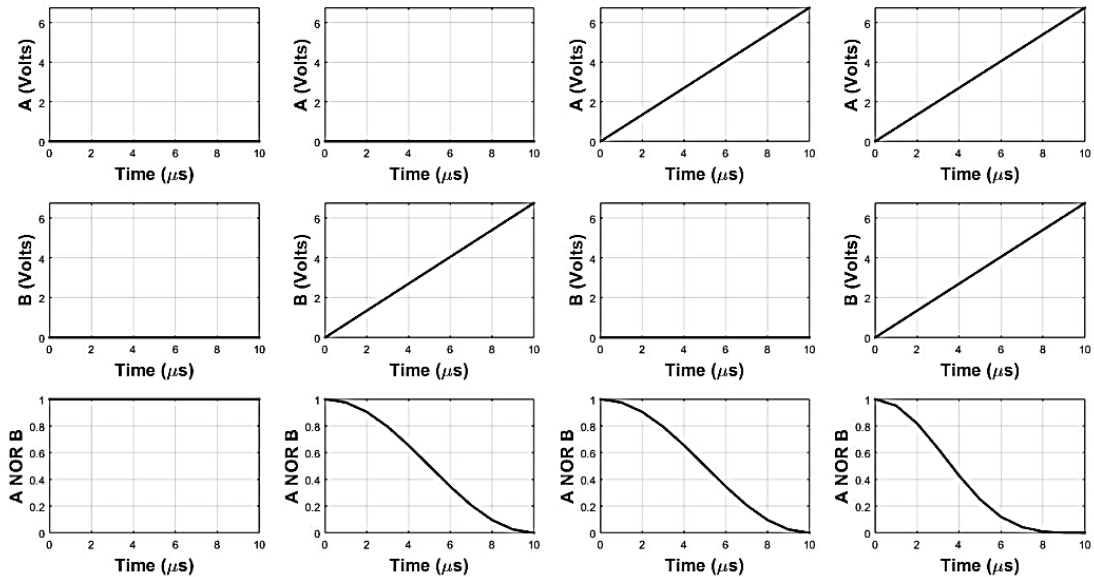
Figure 4.8: MATLAB Simulation results of implemented NOR Gate using MZI's

4.5 NAND GATE

Figure 4.9 depicts the layout used to structure the proposed NAND Gate. NAND gate gives the output logic 1 when its any of the input are at logic 0, if both inputs are logic 1 then the output will be logic 0.
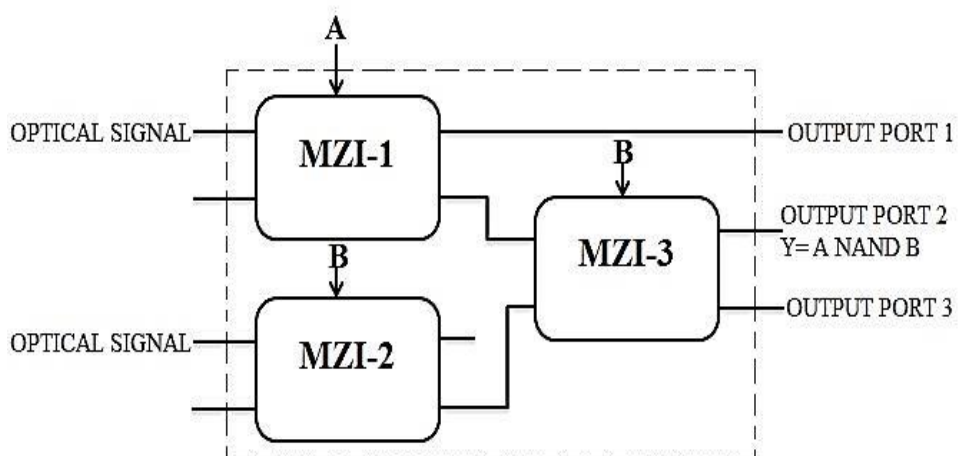
Figure 4.9: Block diagram of NAND Gate

Mathematical equation for normalized power of MZI single staged circuit can be effectively used for normalized power evaluation at the output port of MZI-3. In this

work as shown in figure output ports 3 (Fig.4.9) has been used for evaluation. The output power at the output port can be evaluated utilizing following equations [11]:

$$m_0 = \left|\frac{OUT1_{MZI3}}{E_{in}}\right|^2 = \cos^2\left(\frac{\Delta\varphi_{MZI1}}{2}\right)\cos^2\left(\frac{\Delta\varphi_{MZI2}}{2}\right)\cos^2\left(\frac{\Delta\varphi_{MZI3}}{2}\right) \tag{4.15}$$

$$m_1 = \left|\frac{OUT1_{MZI3}}{E_{in}}\right|^2 = \cos^2\left(\frac{\Delta\varphi_{MZI1}}{2}\right)\sin^2\left(\frac{\Delta\varphi_{MZI2}}{2}\right)\sin^2\left(\frac{\Delta\varphi_{MZI3}}{2}\right) \tag{4.16}$$

$$m_2 = \left|\frac{OUT1_{MZI3}}{E_{in}}\right|^2 = \sin^2\left(\frac{\Delta\varphi_{MZI1}}{2}\right)\cos^2\left(\frac{\Delta\varphi_{MZI2}}{2}\right)\cos^2\left(\frac{\Delta\varphi_{MZI3}}{2}\right) \tag{4.17}$$

Eqs. (4.15)-(4.17) are solved using the assumptions given below [11],

$$\left.\begin{aligned} \Delta\varphi_{MZI1} &= \frac{\pi}{V_\pi}A \\ \Delta\varphi_{MZI2} &= \frac{\pi}{V_\pi}B \\ \Delta\varphi_{MZI3} &= \frac{\pi}{V_\pi}B \end{aligned}\right\} \tag{4.18}$$

Signal A is controlling MZI-1 and Signal B is controlling MZI-2 and MZI-3. At second electrode of each MZI, logic 0 is represented by 0.00V and logic 1 is represented by 6.75V. Hence following expressions for output of the proposed NAND gate can be obtained as [11]:

$$\text{Output port 3 (OR logic)} = \left|\frac{OUT1_{MZI2}}{E_{in}}\right|^2 = m_0 + m_1 + m_2$$

$$= \cos^2\left(\frac{\Delta\varphi_{MZI1}}{2}\right)\cos^2\left(\frac{\Delta\varphi_{MZI2}}{2}\right)\cos^2\left(\frac{\Delta\varphi_{MZI3}}{2}\right)$$

$$+\cos^2\left(\frac{\Delta\varphi_{MZI_1}}{2}\right)\sin^2\left(\frac{\Delta\varphi_{MZI_2}}{2}\right)\sin^2\left(\frac{\Delta\varphi_{MZI_3}}{2}\right)$$

$$+\sin^2\left(\frac{\Delta\varphi_{MZI1}}{2}\right)\cos^2\left(\frac{\Delta\varphi_{MZI2}}{2}\right)\cos^2\left(\frac{\Delta\varphi_{MZI3}}{2}\right) \tag{4.19}$$

Implementation of NAND Gate using MATLAB

To implement the NAND gate three MZI's were used, as represented in Fig. 4.9. At the input of MZI-1 and MZI-2 the optical signal is applied and one of the output port, cross port of MZI-1 is connected to the first input port of MZI-3 and bar port in not connected further. The cross port of MZI-2 is connected to the second input port of MZI-3. The output port 1 of MZI-3 is taken as output of NAND gate shown in the figure. Fig.4.10 shows the results of MATLAB analysis of the implemented NAND gate. The first and second rows in Fig.4.10 represent the input control signals A and B

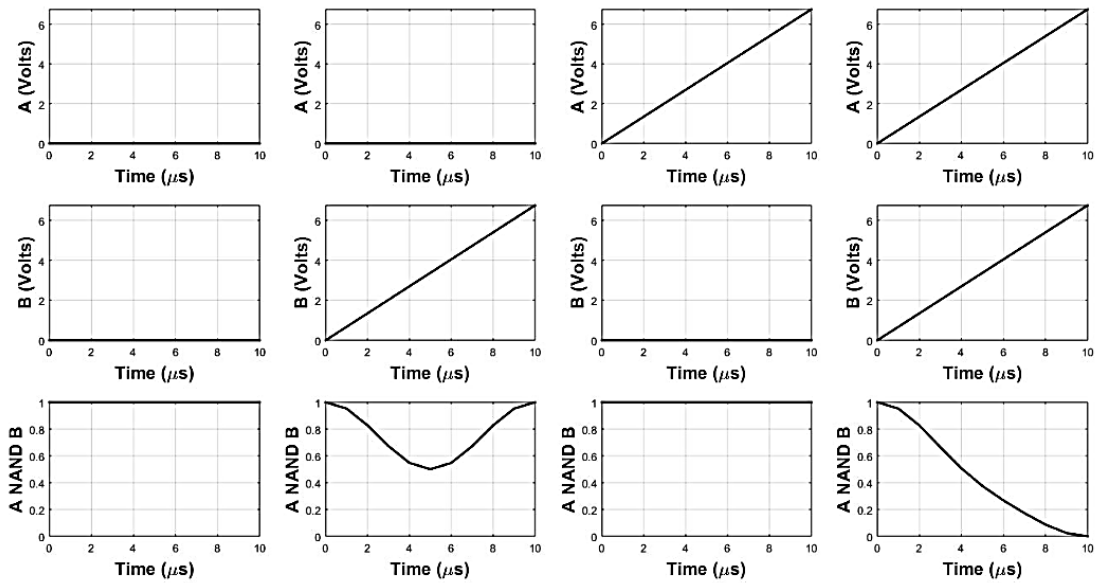respectively used in the simulation. The third row denotes the outputs obtained which is the NAND operation.

Figure 4.10: MATLAB Simulation results of implemented NAND Gate using MZI's

4.6 XOR GATE

Figure 4.11 depicts the layout used to structure the proposed XOR Gate. XOR gate gives logic 1 when odd number of inputs are logic 1 and when even number of inputs are logic 1 then output will be logic 0.

Figure 4.11: Block diagram of XOR Gate

Mathematical equation for normalized power of MZI single staged circuit can be effectively used for normalized power evaluation at the output port of MZI-2. In this work as shown in figure output ports 2 (Fig.4.11) has been used for evaluation. The output power at the output port can be evaluated utilizing following equations:

$$m_1 = \left| \frac{\text{OUT2}_{MZI2}}{\text{E}_{in}} \right|^2 = \cos^2\left(\frac{\Delta\varphi_{MZI1}}{2}\right) \sin^2\left(\frac{\Delta\varphi_{MZI2}}{2}\right) \tag{4.20}$$

$$m_2 = \left| \frac{\text{OUT2}_{MZI2}}{\text{E}_{in}} \right|^2 = \sin^2\left(\frac{\Delta\varphi_{MZI1}}{2}\right) \cos^2\left(\frac{\Delta\varphi_{MZI2}}{2}\right) \tag{4.21}$$

Eqs. (4.20)-(4.21) are solved using the assumptions given below,

$$\Delta\varphi_{MZI1} = \frac{\pi}{V_\pi}A$$

$$\Delta\varphi_{MZI2} = \frac{\pi}{V_\pi}B \qquad \Bigg\} \qquad (4.22)$$

Signal A is controlling MZI-1 and Signal B is controlling MZI-2. At second electrode of each MZI, logic 0 is represented by 0.00V and logic 1 is represented by 6.75V. Hence following expressions for output of the proposed XOR gate can be obtained as:

$$\text{Output port 2 (XOR logic)} = \left|\frac{OUT1_{MZI2}}{E_{in}}\right|^2 = m_1 + m_2$$

$$= \cos^2\left(\frac{\Delta\varphi_{MZI1}}{2}\right)\sin^2\left(\frac{\Delta\varphi_{MZI2}}{2}\right) + \sin^2\left(\frac{\Delta\varphi_{MZI1}}{2}\right)\cos^2\left(\frac{\Delta\varphi_{MZI2}}{2}\right) \qquad (4.23)$$

Implementation of XOR Gate using MATLAB

To implement the XOR logic two MZI's were used, as represented in Fig. 4.11. At the input of MZI-1 the optical signal is applied and its both output ports as shown in the figure are connected directly to MZI-2 input ports. In MZI-2, the one of the output port, the cross port is taken as the output XOR operation. Fig. 4.12 shows the results of MATLAB analysis of the implemented half adder. The first and second rows in Fig. 4.12 represent the input control signals A and B respectively used in the simulation. The third row denotes the outputs obtained which is XOR operations.

Figure 4.12: MATLAB Simulation results of implemented XOR Gate using MZI's

4.7 XNOR GATE

Figure 4.13 depicts the layout used to structure the proposed XNOR Gate. XNOR gate gives logic 1 when its both inputs are same, if inputs are different then output will be logic 0.
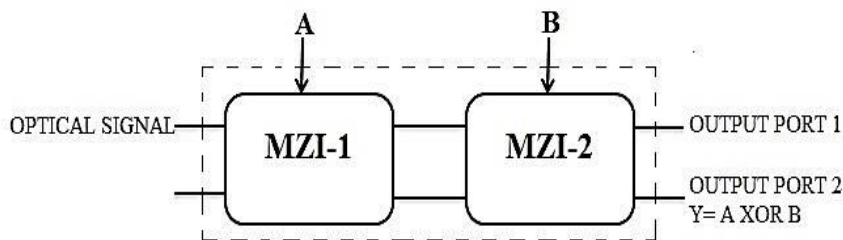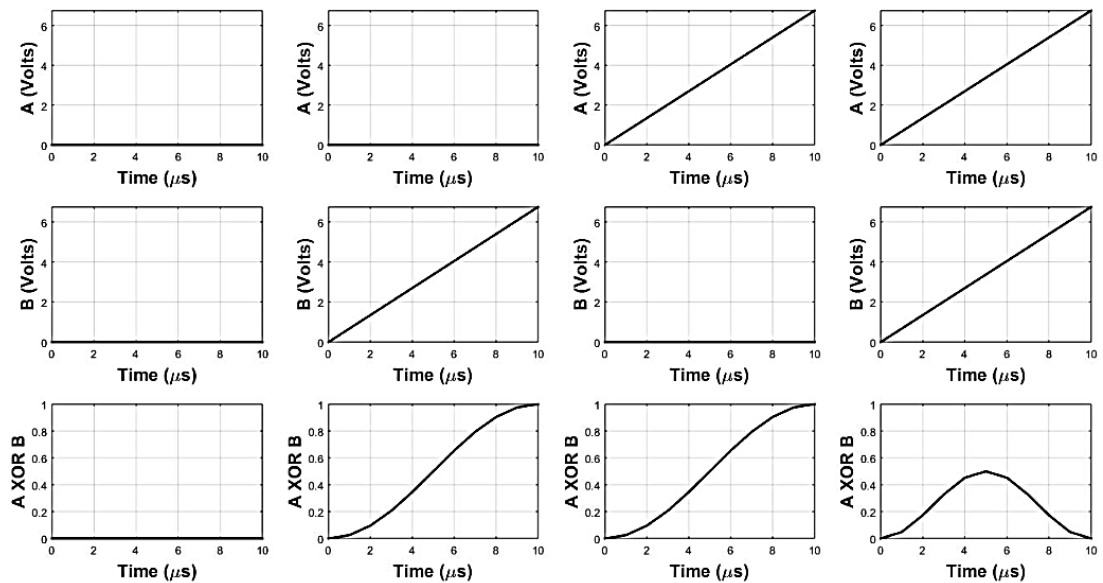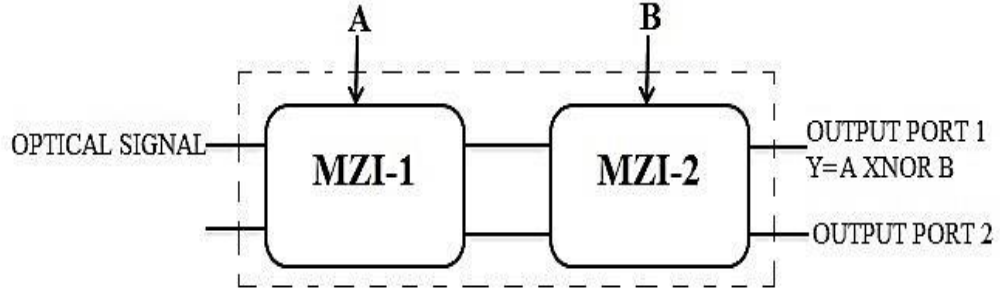

Figure 4.13: Block diagram of XNOR Gate

Mathematical equation for normalized power of MZI single staged circuit can be effectively used for normalized power evaluation at the output port of MZI-2. In this work as shown in figure output ports 2 (Fig.4.13) has been used for evaluation. The output power at the output port can be evaluated utilizing following equations:

$$m_0 = \left| \frac{OUT2_{MZI2}}{E_{in}} \right|^2 = \cos^2\left(\frac{\Delta\varphi_{MZI1}}{2}\right)\cos^2\left(\frac{\Delta\varphi_{MZI2}}{2}\right) \qquad (4.24)$$

$$m_3 = \left| \frac{OUT2_{MZI2}}{E_{in}} \right|^2 = \sin^2\left(\frac{\Delta\varphi_{MZI1}}{2}\right)\sin^2\left(\frac{\Delta\varphi_{MZI2}}{2}\right) \qquad (4.25)$$

Eqs. (4.24)-(4.25) are solved using the assumptions given below,

$$\left.\begin{array}{l} \Delta\varphi_{MZI1} = \frac{\pi}{V_\pi}A \\[2mm] \Delta\varphi_{MZI2} = \frac{\pi}{V_\pi}B \end{array}\right\} \qquad (4.26)$$

Signal A is controlling MZI-1 and Signal B is controlling MZI-2. At second electrode of each MZI, logic 0 is represented by 0.00V and logic 1 is represented by 6.75V. Hence following expressions for output of the proposed NAND gate can be obtained as:

Output port 1 (XNOR logic) $= \left| \frac{OUT1_{MZI2}}{E_{in}} \right|^2 = m_0 + m_3$

$$= \cos^2\left(\frac{\Delta\varphi_{MZI1}}{2}\right)\sin^2\left(\frac{\Delta\varphi_{MZI2}}{2}\right) + \sin^2\left(\frac{\Delta\varphi_{MZI1}}{2}\right)\cos^2\left(\frac{\Delta\varphi_{MZI2}}{2}\right) \qquad (4.27)$$

Implementation of XNOR logic using MATLAB

To implement the XNOR logic two MZI's were used, as represented in Fig. 4.13. At the input of MZI-1 the optical signal is applied and its both output ports as shown in the figure are connected directly to MZI-2 input ports. In MZI-2, the one of the output port, the bar port is taken as the output XNOR operation. Fig. 4.14 shows the results of MATLAB analysis of the implemented half adder. The first and second rows in Fig. 4.14 represent the input control signals A and B respectively used in the simulation. The third row denotes the outputs obtained which is an XNOR operation.
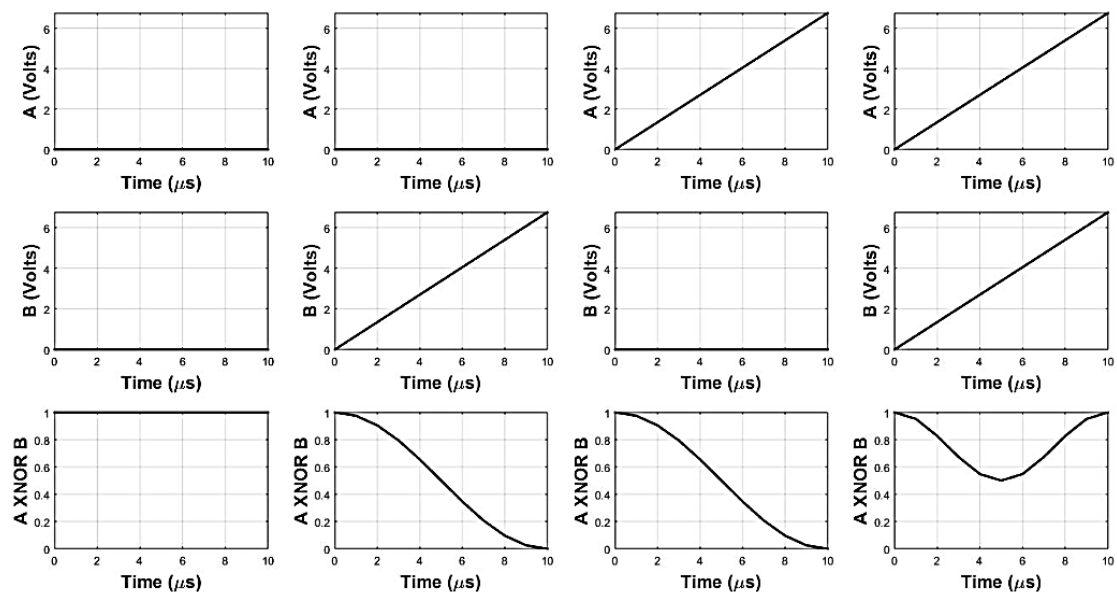
Figure 4.14: MATLAB Simulation results of implemented XNOR Gate using MZI's

4.8 HALF ADDER

Figure 4.15 depicts the layout used to structure the proposed half adder. Half adder is a combinational circuit in digital electronics which adds two, one bit binary digits and generates two bits where one bit is sum, obtained by XOR operation and the other is carry bit generated by AND operation.
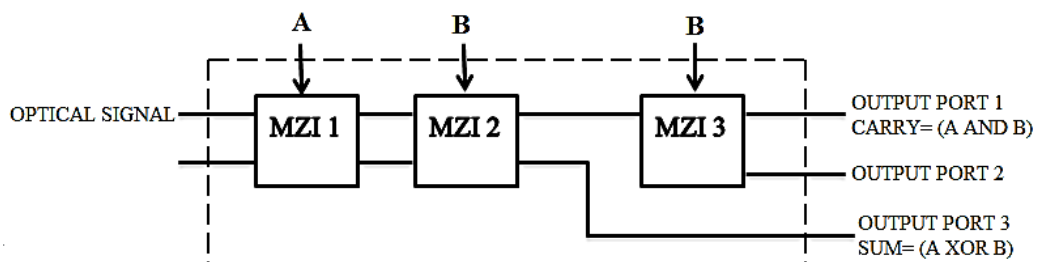

Figure 4.15: Block diagram of Half Adder

Mathematical equation for normalized power of MZI single staged circuit can be effectively used for normalized power evaluation at the output ports of MZI-2 and MZI-3 [3-4]. In this work as shown in figure output ports 3 and 1 (Fig.4.15) respectively has been used for evaluation. The output power at both the output ports can be evaluated utilizing following equations:

$$m_1 = \left|\frac{OUT2_{MZI2_1}}{E_{in}}\right|^2 = \cos^2\left(\frac{\Delta\varphi_{MZI1}}{2}\right)\sin^2\left(\frac{\Delta\varphi_{MZI2}}{2}\right) \qquad (4.28)$$

$$m_2 = \left|\frac{OUT2_{MZI2_2}}{E_{in}}\right|^2 = \sin^2\left(\frac{\Delta\varphi_{MZI1}}{2}\right)\cos^2\left(\frac{\Delta\varphi_{MZI2}}{2}\right) \qquad (4.29)$$

$$m_3 = \left|\frac{OUT1_{MZI3}}{E_{in}}\right|^2 = \sin^2\left(\frac{\Delta\varphi_{MZI1}}{2}\right)\sin^2\left(\frac{\Delta\varphi_{MZI2}}{2}\right)\sin^2\left(\frac{\Delta\varphi_{MZI3}}{2}\right) \qquad (4.30)$$

Eqs. (4.28)-(4.30) are solved using the assumptions given below,

$$\left.\begin{array}{l} \Delta\varphi_{MZI_1} = \dfrac{\pi}{V_\pi}A \\[3mm] \Delta\varphi_{MZI_2} = \dfrac{\pi}{V_\pi}B \\[3mm] \Delta\varphi_{MZI_3} = \dfrac{\pi}{V_\pi}B \end{array}\right\} \qquad (4.31)$$

Signal A is controlling MZI-1 and Signal B is controlling MZI-2 and MZI-3. At second electrode of each MZI, logic 0 is represented by 0.00V and logic 1 is represented by 6.75V. Hence following expressions for sum and carry of the proposed half adder can be obtained as:

Output port 3 (XOR logic for sum of half adder) $= \left|\dfrac{OUT1_{MZI2}}{E_{in}}\right|^2 = m_1 + m_2$

$$= \cos^2\left(\frac{\Delta\varphi_{MZI1}}{2}\right)\sin^2\left(\frac{\Delta\varphi_{MZI2}}{2}\right) + \sin^2\left(\frac{\Delta\varphi_{MZI1}}{2}\right)\cos^2\left(\frac{\Delta\varphi_{MZI2}}{2}\right) \qquad (4.32)$$

Output port 1 (AND logic for carry of half adder) $= \left|\dfrac{OUT1_{MZI3}}{E_{in}}\right|^2 = m_3$

$$= \sin^2\left(\frac{\Delta\varphi_{MZI1}}{2}\right)\sin^2\left(\frac{\Delta\varphi_{MZI2}}{2}\right)\sin^2\left(\frac{\Delta\varphi_{MZI3}}{2}\right) \qquad (4.33)$$

Implementation of Half Adder using MATLAB

To implement the half adder three MZI's were used, as represented in Fig. 4.15. At the input of MZI-1 the optical signal is applied and its both output ports as shown in the figure are connected directly to MZI-2 input ports. In MZI-2, the one of the output port, the bar port is connected to the first input port of MZI-3 and other, the cross port

is taken as the output port of the circuit giving the resultant sum of the half adder circuit implemented (XOR operation). The carry generated by the circuit can be obtained at bar port as shown in the figure which is the first output port of MZI-3. Fig. 4.16 shows the results of MATLAB analysis of the implemented half adder. The first and second rows in Fig. 4.16 represent the input control signals A and B respectively used in the simulation. The third and fourth row denotes the outputs obtained which are the sum and carry obtained through XOR and AND operations.
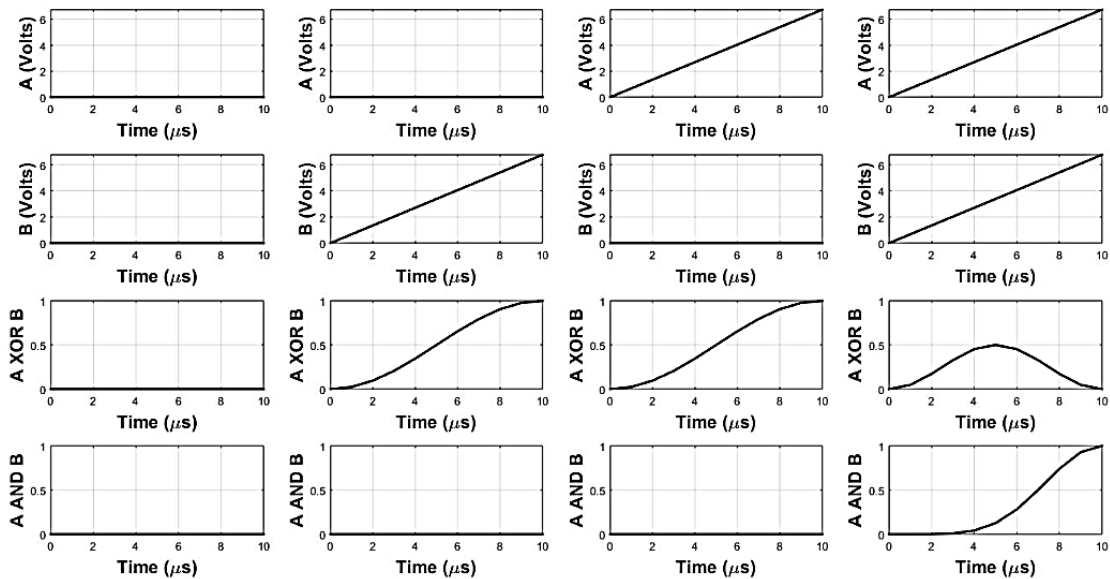

Figure 4.16: MATLAB Simulation results of implemented Half Adder using MZI's

CHAPTER 5: OPTI-BPM TOOL

5.1 Introduction

In this chapter, there is brief discussion about OPTI-BPM simulator tool. Expanded form of name OptiBPM is Optical Beam Propagation Method. For various embedded and fiber optics, BPM which is strong and user friendly software, gives a platform for designing wave issue on our desktop. "Beam Propagation Method (BPM) is a method of simulating in which device simulate step-by-step as light passes through any waveguide medium". As an optical signal propagates along a waveguide design, an optical field can be verified at any level. BPM allows computer-simulated analysis of the distribution of light fields. The radiation and the guided field can be observed at a moment. OptiBPM makes it possible to design waveguide equipment with simple data entry. and freely design devices and operate different simulations.

It is possible to simulate an optical signal in OptiBPM in 2D and 3D waveguide devices [23].

- In 2D, X-direction which is vertical, behave as Transverse and Z-direction which is horizontal, behave as Propagation.
- In 3D, X-direction which is vertical, behave as Transverse, Y-direction is behave as Depth and Z-direction which is horizontal, behave as Propagation.

From a real three dimensional device to acquire a 2D device, an effective index method can be implemented. The transverse cross-section of two dimension device is replaced by a cross-section of one-dimensional to achieve a three dimensional device from two dimensional device. One dimension efficient index distribution exchanges the actual index cross-section. While an approximate solution is the efficient index method, it operates for many devices.

All the functions which are needed to design step-index waveguide are provided by beam propagation method in 3D. The data design input comprises of the distribution of refractive index, propagation field for initiation, and numerical parameters set in the three-dimensional beam propagation method. The project's waveguide design offers refraction distribution index. The initial field could be a waveguide mode, Gaussian, rectangular, or a field defined by user provided from a file. There is a Global Data dialog box in which all simulation parameters are specified and this dialog box can be accessed via the Simulation menu. Output information includes many kinds of file that can be shown by other simulations [23].

5.2 Numerical Simulations

The simulating environment for OptiBPM consists of the Beam Propagation Method as the main component, along with mode solvers that match the algorithms of the Beam Propagation Method. BPM's basic concept is mathematical model equation that controls propagation of light in dielectric medium. BPM is related to solving the Helmholtz equation and considers monochromatic signals. The advantage of propagation models based on Helmholtz equation approximations might be – [23]

- reduce complexity of the simulations
- to faster the response
- organize computer memory better

5.3 2D BPM

Crank-Nicolson's unconditionally stable finite difference method algorithm is the fundamental 2D BPM simulator base. Customization of following programme can be done of the following programme option, according to the design – [23]

- Algorithms that give a decision between transverse electrical and transverse magnetic polarization.
- Pade-based wide-angle propagation, Pade (1,1) and (2,2) to (4,4)
- A rectangular field, a Gaussian field or field defined by use are the choice of field as a waveguide mode.
- At an angle initial field could be started.
- Modal, average or user-defined refractive index selection
- Transparent boundary condition (TBC)

5.4 3D BPM

The simulator for 3D beam propagation method is based on ADI scheme, scalar algorithms, a choice provided by Semi-Vector algorithms between quasi TE and quasi TM polarization, and both component transversal fields are governed by Full-Vector algorithms [23].

5.5 Mode solvers

Two and three dimensions algorithm of mode solver is compatible with OptiBPM software. The mode solvers use various techniques that will be for multilayer planar

design that will be TMM, ADI in 2D and 3D respectively and CFM in both dimensions.

The planar structure concept is based on the resolution at dielectric interfaces of different boundary conditions between layers. During the propagation of a user-defined field, the CFM calculates the integral correlation between the input field and the propagation field at each stage. This produces the correlation feature of the field amplitude of the waveguide. The correlation function contains all the data needed to fully describe the fields, including the constant propagation, the weights of every mode, and eigen functions of each mode.

The ADI method divides the derivatives of X and Y into two single iteration phase parts. Due to its rapid convergence, this technique is superior to certain finite-difference methods. All constants of propagation and eigen function mode given by ADI method [23].

5.6 Basic Steps to design a basic Mach Zehnder switch in OPTI-BPM

Details on how to build a design, operate a simulation, view the simulation outcomes and save the design project are given in this chapter. For fast starting settings and values used here. Use the settings and values are require when we creating our own projects [24].

The following applications are available in OptiBPM -

- OptiBPM Layout Designer
- Profile Designer
- OptiBPM Simulator
- OptiBPM Analyzer

To get started, a design project will be generated in the Designer and project will be saved as a .bpd file.

In the OPTI-BPM official website, all processes are described in detail. But these steps are briefly described below and can be referred to this for thorough knowledge of OPTI-BPM. Here, the built-in switch is supposed to be built on a Lithium Niobate z-cut wafer and enclosed by air cladding. The structure is oriented in the direction of Lithium Niobate's Y-optical axis. We therefore need to identify a diffused substrate material and a dielectric cladding material.

A tool used in embedded fiber optics is an EO switch. For MZI, a substrate is made up of Titanium diffused Lithium Niobate. By the electro-optic effect switching

is done in the proposed structure. The electric field is distributed in structure by applying voltage in the electrode region of MZI which results into change in its refractive index. If design is perfect then change in refractive index results into distinct coupling between ports.

Designing procedure steps are as following: [24]

- Layout of CAD design
- Describing the materials
- Defining the profile of Ti-diffusion
- Creating the Wafer
- Describing the device
- Creating the region of electrode
- Creating the input plane and parameters of simulation
- Simulation

Layout of CAD design

We imagine the embedded switch will be produced on a Lithium Niobate z-cut wafer and will be enclosed by air cladding. The structure is oriented in the direction of Lithium Niobate's Y-optical axis. We therefore need to identify a diffused substrate material and a dielectric cladding material.

Describing the materials

Step 1: In the Layout Designer open a new project then dialog box of Initial Properties is pop up.

Step 2: To open the Profile Designer click on the profiles and materials and following diffused material is created that is Lithium_Niobate is the name of crystal, z is the Crystal cut and y is the propagation direction. Then following dielectric material is defined that is Name is air and Refractive Index is 1.

Defining the profile of Ti-diffusion

Step 3: Define Profile name is TiLiNbO3 Pro 1 in the Profile Designer.

Step 4: In the Profile Designer select Group I panel then define 3.5 µm Lateral Diffusion length and 4.2 µm is Diffusion length in Depth. After that Profile Designer is closed and Layout Design is appeared.
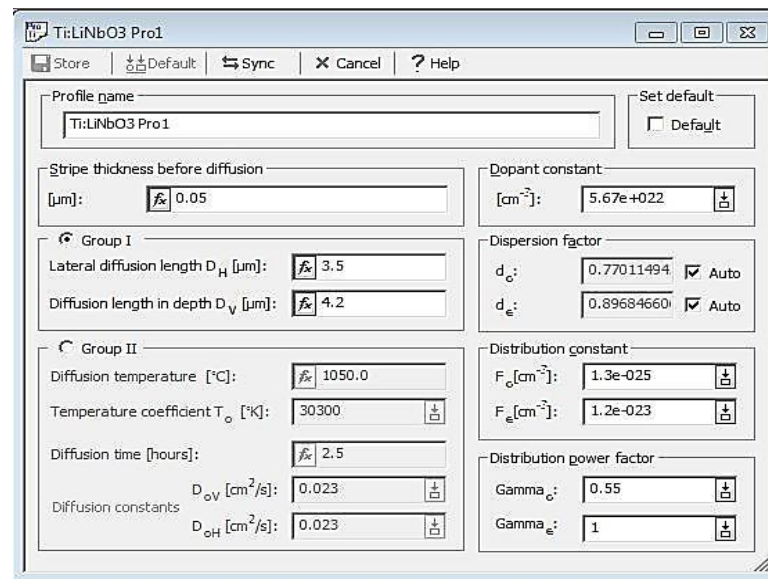
Figure 5.1: Dialog box of Profile Designer

Creating the Wafer

Step 5: Waveguide Properties tab open in Initial Properties dialog box and define Width is 8.0 µm and Profile is TiLiNbO3 Pro 1.

Step 6: After that Wafer Dimension tab is open and define wafer length is 33000 µm and wafer width is 100 µm.

Step 7: Then 2D Wafer properties tab is open and define Wafer Refractive Index Material is Lithium_Niobate.

Step 8: After that 3D Wafer Properties tab is open and defines air is the material of cladding, 2 µm is the thickness of cladding, Lithium_Niobate is the material of substrate and 10 µm is the thickness of substrate. Then to save all settings click OK.

Describing the device

Step 8: To see the whole substrate, following setting will done as select Preference>Layout Options> Display ratio, and enter 200.

In designing of MZI through selecting different waveguides with different shapes like here we use SBendSin waveguide which is curved shape and Linear waveguide which is straight. Table 5.1 describe the horizontal and vertical dimensions of each SBendSin and Linear waveguide.

Table 5.1: Create waveguides in Layout Designers [24]:

Name of Waveguide	Horizontal Start Position	Vertical Start Position	Horizontal End Position	Vertical End Position
SBendSin1	0	-20	5750	-7.25
Linear1	5750	-7.25	9000	-7.25
SBendSin2	9000	-7.25	11500	-116
Linear2	11500	-16	21500	-16
SBendSin3	21500	-16	24000	-7.25
Linear3	24000	-7.25	27250	-7.25
SBendSin4	27250	-7.25	33000	-20

 Step 9: Select all the waveguide on the layout.

Step 10: To create the top waveguides mirror and flip operations is perform by Edit > Flip and Mirror > Mirror to top menu. By this a duplicate waveguides is obtained above the selected waveguide.

Step 11: After that open the properties dialog box by double-clicking on the each waveguide and enter the x-coordinates values in the horizontal coordinate which remains same and vertical coordinates which is reverse sign of its counterpart of selected waveguide
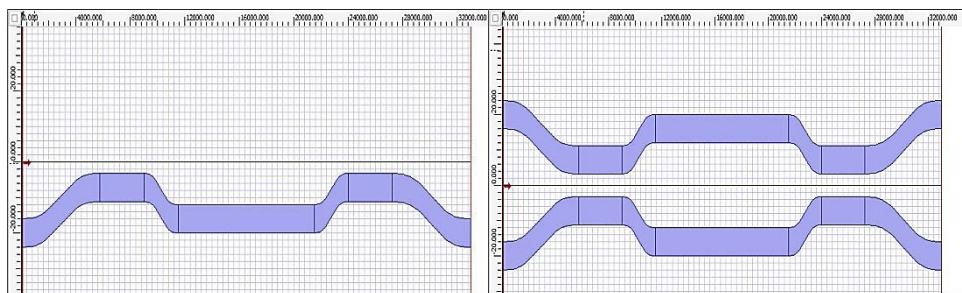

Figure 5.2: Waveguide design on Layout

Perform the following steps to check RI profile for selection of z- distance of x-y slice:

Step 12: Choose the Ref. Index (n)–On the bottom of the design designer window, the 3D XY Plane view tab. Then select Z distance from Select Preference > Refractive Index View > 3D Slice (XY Plane) > Select Z Distance.

Step 13: Dialog box of XY Refractive Index view option is pop up in which enter Z distance value and click on view. By this Z distance is updated.
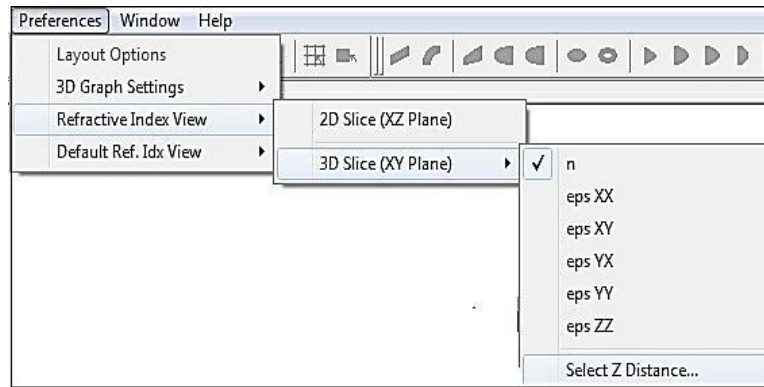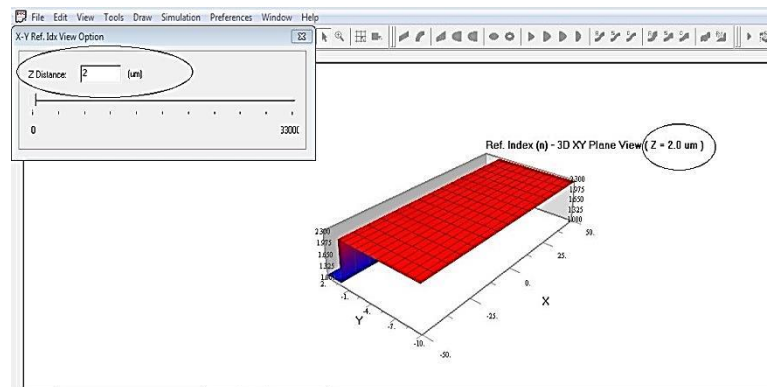
Figure 5.3: Steps for selecting Z distance

Figure 5.4: Refractive Index view in which Z distance is entered

Creating the region of electrode

Step 14: To select electrode region go through as Select Draw > Regions > Electrode Region.

Step 15: After that click and move the mouse where we draw the electrode region on the layout. Electrode region is drawn.

Step 16: Double click on electrode region then dialog box is pop up where we enter start and end positions 11500 µm and 21500 µm respectively of the electrode region.
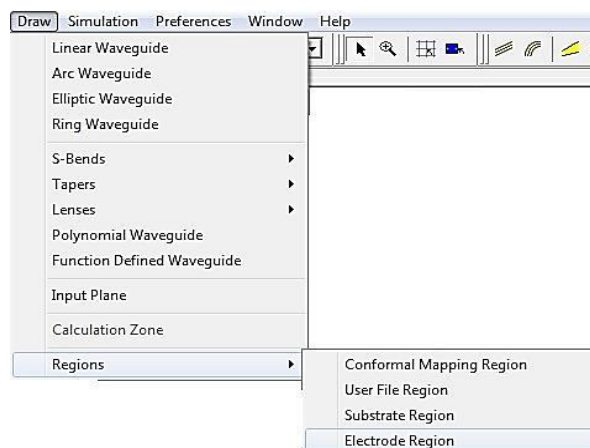

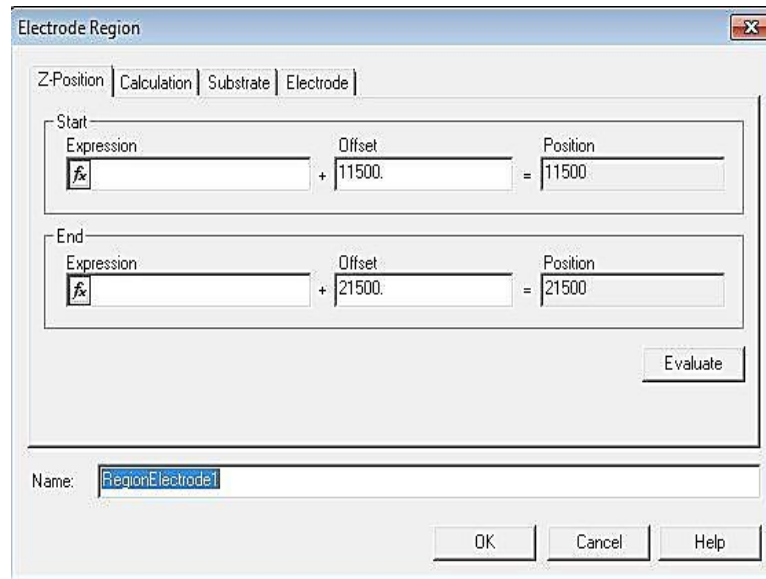**Figure 5.5:** Steps for selecting Electrode Region

Figure 5.6: Dialog box in which define length of electrode region

Step 17: In electrode tab, buffer layer properties can be defined to build electrode on the top of buffer layer.

Step 18: For defining buffer layer select All sets > Electrode with buffer layer where on 0.3 µm is the thickness of Buffer layer, 4 is the horizontal permittivity and vertical permittivity, 4 µm is the thickness of electrode and material is buffer.

Step 19: Click on material in use for defining the new dielectric material in Profile Designer, where enter the name is Buffer and Refractive Index is 1.47.

Step 20: For Electrode Set dialog box , under Electrode sets table, click Add and then in Electrode 1 enter width is 50 and voltage is 0.0, in Electrode 2 enter width is 26 and voltage is 0.0, in Electrode 3 enter width is 50 and voltage is 0.0, gap 1-2 is 6.0, gap 2-3 is 6.0 and last center position of Electrode 2 is 5.5. At last close all the dialog boxes.
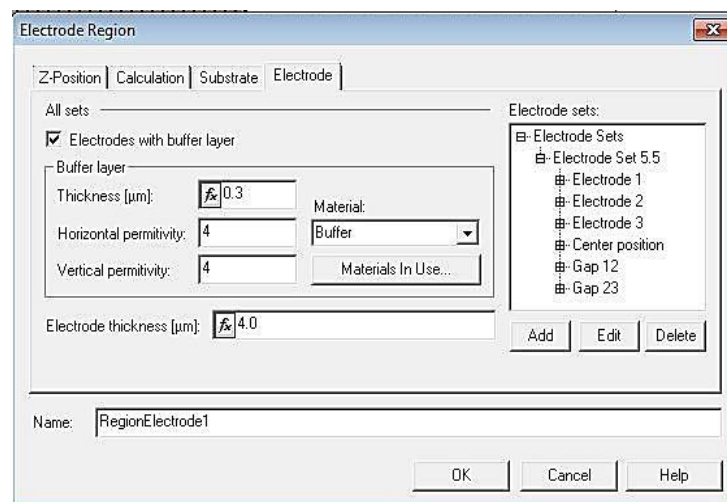

Figure 5.7: Defining electrodes with Buffer layer

We defined an electrode region with three electrodes, all with zero voltage, slightly off the Mach-Zehnder interferometer's symmetry axis.

Figure 5.8: Define electrode set

Creating the input plane and parameters of simulation

Step 21: To draw input plane select Draw > Input plane in the layout.

Step 22: In the dialog box of the Input Plane properties enter starting field is Mode, Z position offset is 0.0, then open 2D input field tab > click edit and dialog box of input field is pop up, after that select second waveguide and click on Add in waveguide table and this entry is appear in field table, then close all dialog box.

Step 23: Performing the simulation we select Simulation > Simulation parameter and dialog box is pop up. In this dialog box, Global Data tab enter Reference Index is Modal and Wavelength is 1.33 µm.

Step 24: In 2D tab enter Polarization is TM, number of points of mesh is 500, BPM solver is paraxial, finite difference engine, 0.5 is the scheme parameter, Propagation Step is 1.3 and choose Transparent Boundary Condition (TBC). Then close all dialog boxes.

Simulation

Step 25: To perform simulation, select Simulation > Calculate 2D Isotropic Simulation and dialog box appears, then click on Run and OptiBPM Simulator 2D is open.

Step 26: Simulation is Run for two values of voltage 0.0 (logic 0) and 6.75 (logic 1) and this voltage is changed by the central electrode voltage in Electrode Region dialog box, click on Edit and enter the values 0.0 or 6.75 in Electrode 2 – Voltage (V).
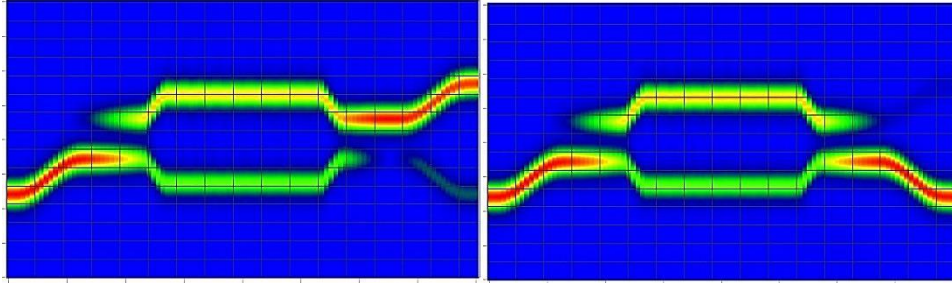

Figure 5.9: Simulation results of MZI

CHAPTER 6: PROPOSED DESIGNS OF OPTICAL LOGIC GATES AND HALF ADDER

In this chapter optical logic gates and half adder is discussed. Designs which I have developed are given in details with the simulation results and required parameters. By using these results, Insertion Loss and Extinction Ratio of designs are calculated. These circuits designed using OptiBPM software which is explained in chapter 4. We have discussed about logic gates and half adder designs which shows the high value of extinction ratio along with the small value of insertion loss.

- NOT Gate
- AND Gate
- OR Gate
- NOR Gate
- NAND Gate
- XOR Gate
- XNOR Gate
- Half Adder

Detailed explanation of each design is given in the following subsection with important parameters like Insertion Loss and Extinction Ratio Calculation.

6.1 NOT Gate

To implement the NOT gate single MZI was used, as represented in Fig. 4.1. At the input of MZI-1 the optical signal is applied and at cross port is taken as output of NOT gate shown in the figure. Fig. 6.1 shows the structure of the implemented NOT gate using OptiBPM.
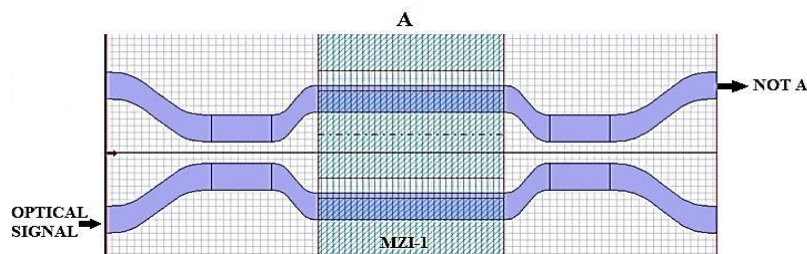

Figure 6.1: Layout structure of NOT Gate

The results of simulation using BPM is shown in Fig. 6.2, where the NOT gate is seen to give acceptable results through proper selection of control signal. The operating

principle of the proposed structure can be well monitored using the truth table, Table. 6.1. The results of simulation based analysis has been compared with the BPM results for its validation and verification as shown in Fig. 6.2

Table 6.1: Input and output of NOT Gate layout

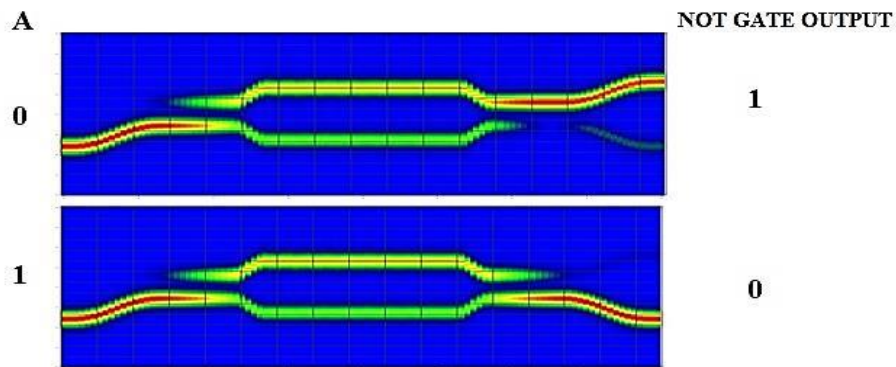| Control/Input Signal	Outputs	
A	Port 1 (C = NOT A)	Port 2
0	1	0
1	0	1

Figure 6.2: Results of NOT Gate using beam propagation method

Impact of Ti strip thickness on IL and ER

In this, impact of Ti strip thickness on power performance of the NOT gate has been investigated by varying the thickness of Ti strip from 0.05 µm to 0.09 µm and plot the graph between the extinction ratio and the thickness of titanium strip and insertion loss and thickness of titanium strip. And we obtain the highest value 28.68 dB of extinction ratio and lowest value of insertion loss 0.050 dB at the 0.05 µm thickness and we increase or decrease the titanium thickness the extinction ratio will be low and insertion ratio will be high.
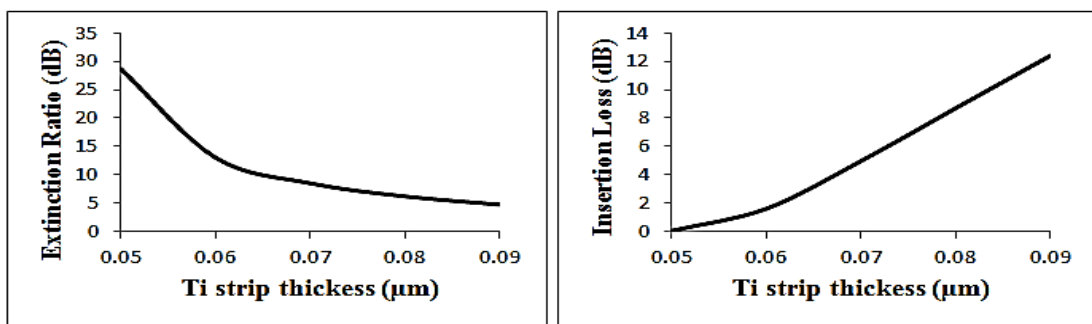

(a)   (b)

Figure 6.3: (a) Variation of ER with increase in thickness of Ti strip of NOT Gate (b) Variation of IL with increase in thickness of Ti strip of NOT Gate

6.2 AND GATE

To implement the AND gate two MZI's were used, as represented in Fig. 4.3. At the input of MZI-1 the optical signal is applied and bar port of MZI-2 is taken as output of AND gate shown in the figure. Fig. 6.4 shows the structure and results of the implemented AND gate using OptiBPM.
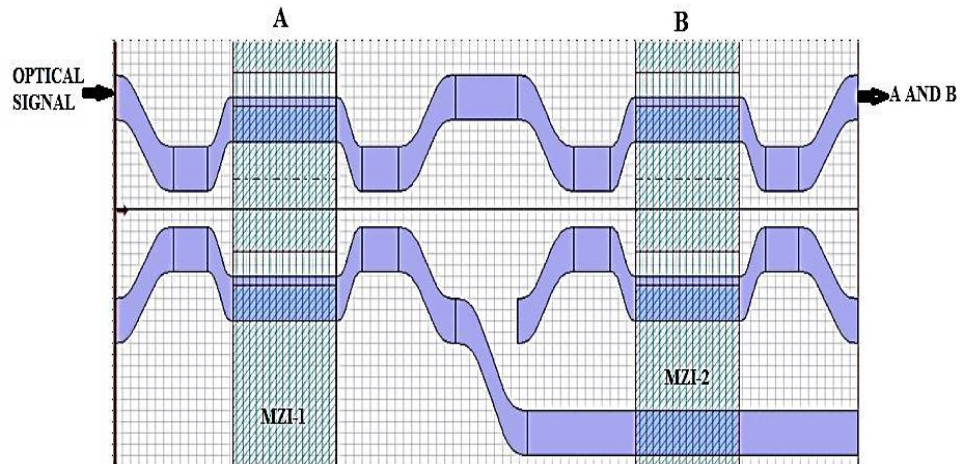

Figure 6.4: Layout structure of AND Gate

The results of simulation using BPM is shown in Fig. 6.5, where the AND gate is seen to give acceptable results through proper selection of control signals. The operating principle of the proposed structure can be well monitored using the truth table, Table. 6.2. The results of simulation based analysis have been compared with the BPM results for its validation and verification as shown in Fig. 6.5.

Table 6.2: Inputs and outputs of AND Gate layout

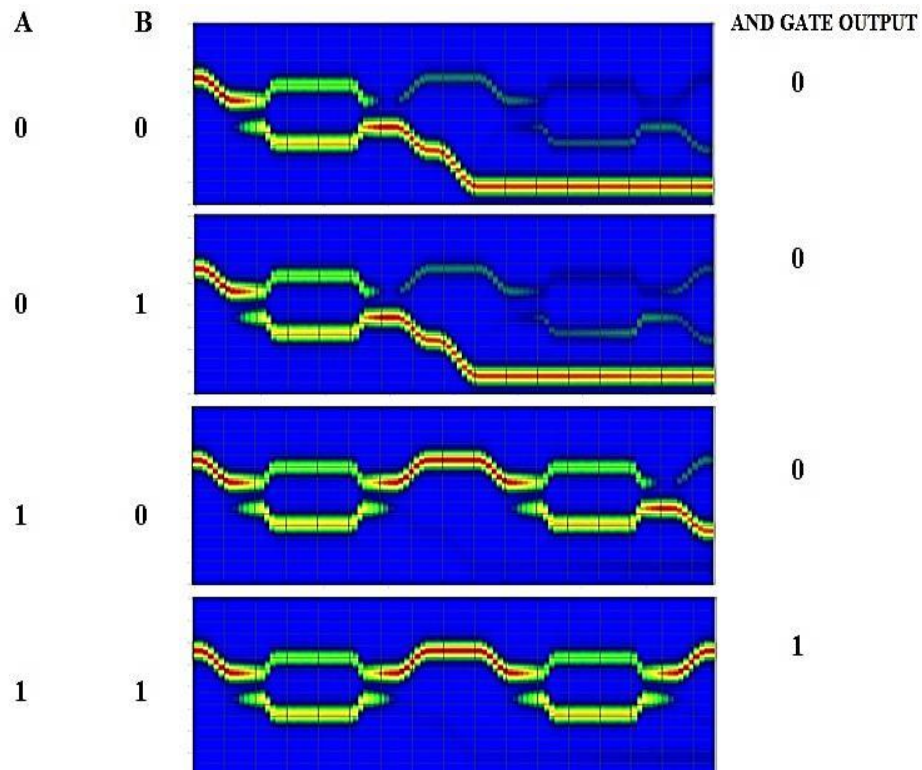| Control/ Input Signals		Outputs		
A	B	Port 1 (C = A AND B)	Port 2	Port 3
0	0	0	0	1
0	1	0	0	1
1	0	0	1	0
1	1	1	0	0

Figure 6.5: Results of AND Gate using beam propagation method

Impact of Ti strip thickness on IL and ER

In this, impact of Ti strip thickness on power performance of the AND gate has been investigated by varying the thickness of Ti strip from 0.05 µm to 0.09 µm and plot the graph between the extinction ratio and the thickness of titanium strip and insertion loss and thickness of titanium strip. And we obtain the highest value 15.13 dB of extinction ratio and lowest value of insertion loss 0.128 dB at the 0.05 µm thickness and we increase or decrease the titanium thickness the extinction ratio will be low and insertion ratio will be high.

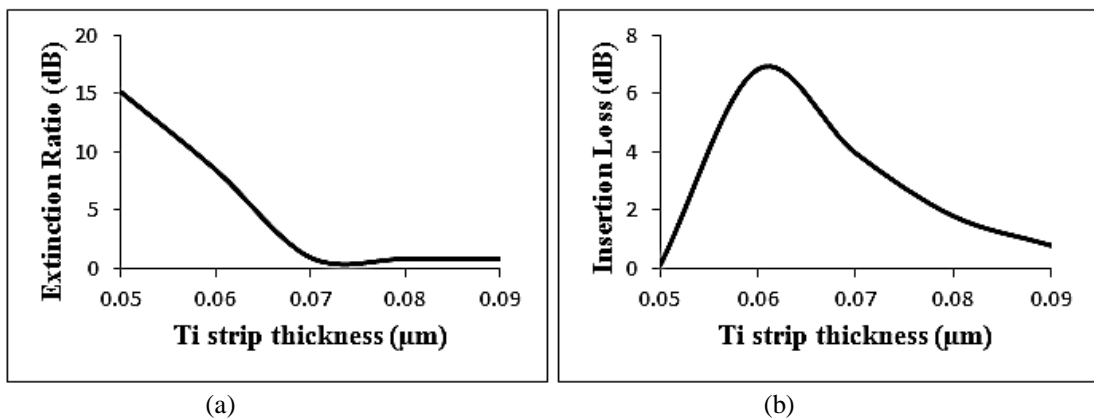(a)   (b)

Figure 6.6: (a) Variation of ER with increase in thickness of Ti strip of AND Gate (b) Variation of IL with increase in thickness of Ti strip of AND Gate

6.3 OR GATE

To implement the OR gate three MZI's were used, as represented in Fig. 4.5. At the input of MZI-1 and MZI-2 the optical signal is applied and second port of MZI-3 is taken as output of OR gate shown in the figure. Fig. 6.7 shows the structure and results of the implemented OR gate using OptiBPM.
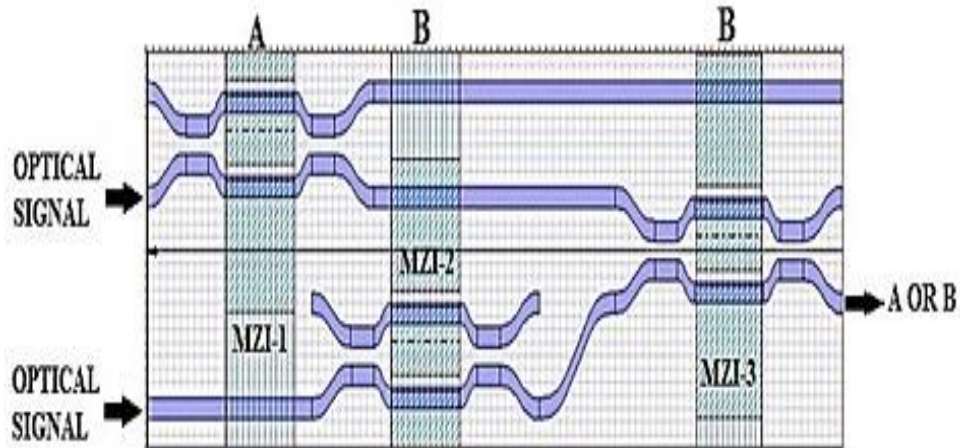

Figure 6.7: Layout structure of OR Gate

The results of simulation using BPM is shown in Fig. 6.8, where the OR gate is seen to give acceptable results through proper selection of control signals. The operating principle of the proposed structure can be well monitored using the truth table, Table. 6.3. The results of simulation based analysis have been compared with the BPM results for its validation and verification as shown in Fig. 6.8.

Table 6.3: Inputs and outputs of OR Gate layout

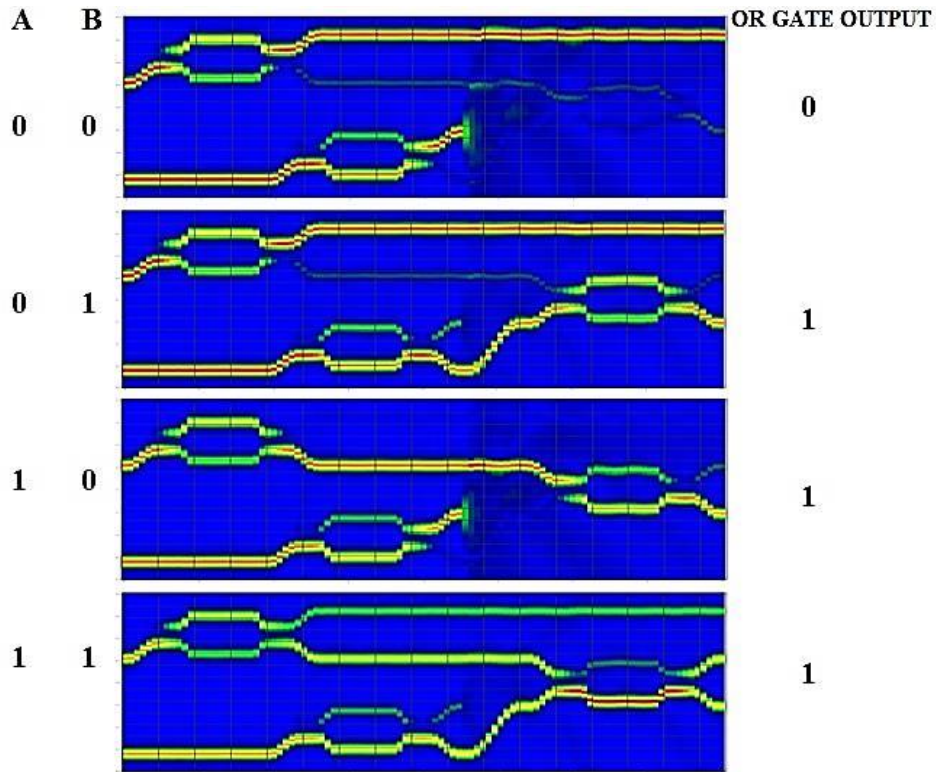| Control/ Input Signals		Outputs		
A	B	Port 1	Port 2	Port 3 (S = A OR B)
0	0	1	0	0
0	1	1	0	1
1	0	0	0	1
1	1	0	1	1

Figure 6.8: Results of OR Gate using beam propagation method

Impact of Ti strip thickness on IL and ER

In this, impact of Ti strip thickness on power performance of the OR gate has been investigated by varying the thickness of Ti strip from 0.05 µm to 0.09 µm and plot the graph between the extinction ratio and the thickness of titanium strip and insertion loss and thickness of titanium strip. And we obtain the highest value 9.332 dB of extinction ratio and lowest value of insertion loss 2.531 dB at the 0.05 µm thickness and we increase or decrease the titanium thickness the extinction ratio will be low and insertion ratio will be high.

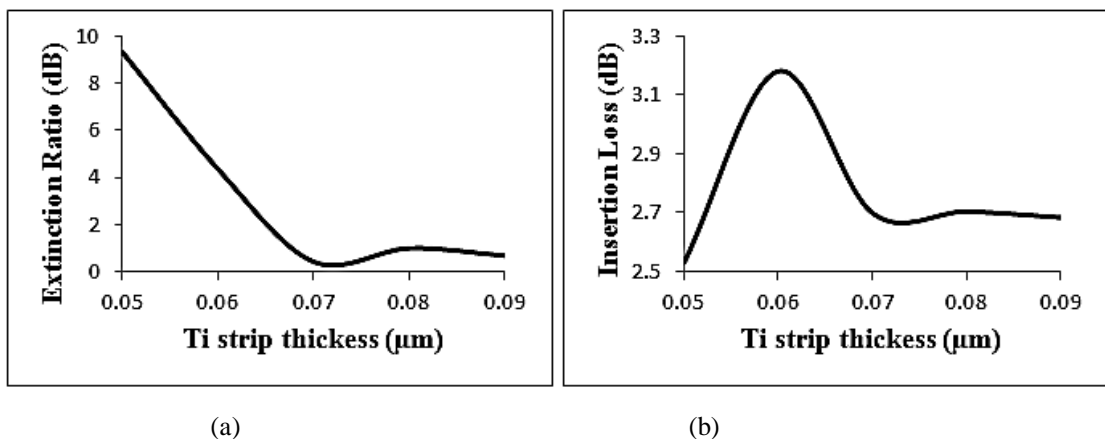(a)   (b)

Figure 6.9: (a) Variation of ER with increase in thickness of Ti strip of OR Gate (b) Variation of IL with increase in thickness of Ti strip of OR Gate

6.4 NOR GATE

To implement the NOR gate two MZI's were used, as represented in Fig. 4.7. At the input of MZI-1 the optical signal is applied and first port of MZI-2 is taken as output of NOR gate shown in the figure. Fig. 6.10 shows the structure and results of the implemented NOR gate using OptiBPM
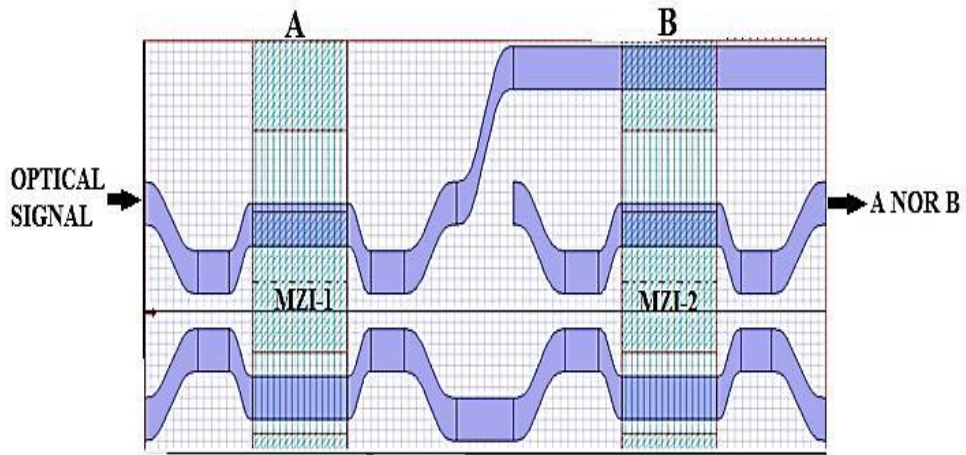

Figure 6.10: Layout structure of NOR Gate

The results of simulation using BPM is shown in Fig. 6.11, where the NOR gate is seen to give acceptable results through proper selection of control signals. The operating principle of the proposed structure can be well monitored using the truth table, Table. 6.4. The results of simulation based analysis has been compared with the BPM results for its validation and verification as shown in Fig. 6.11

Table 6.4: Inputs and outputs of NOR Gate layout

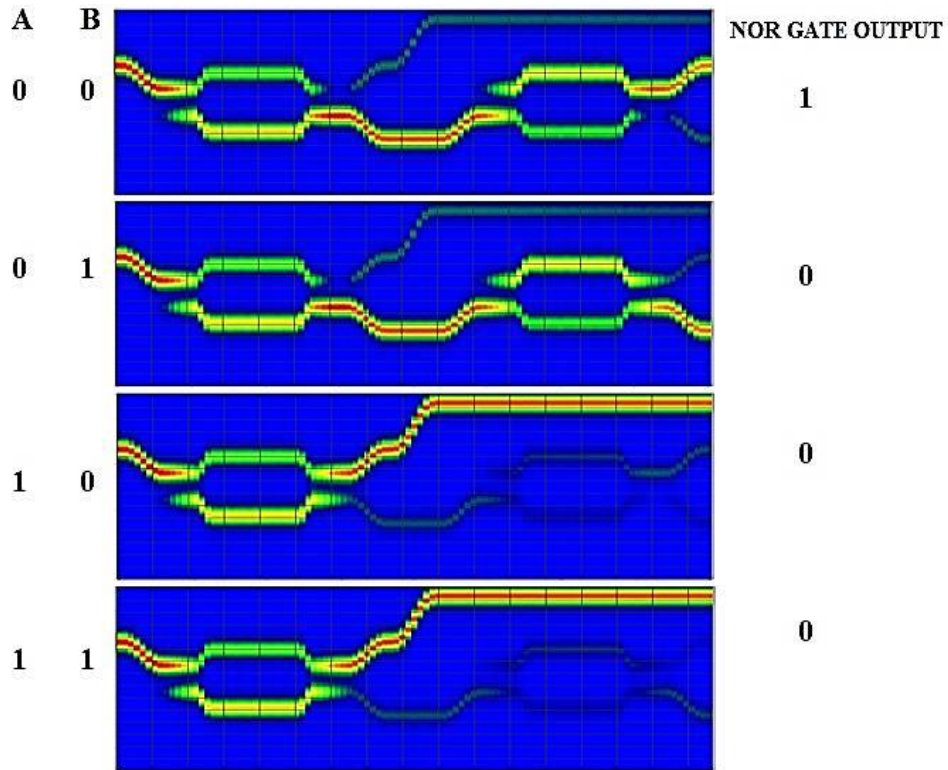| Control/ Input Signals		Outputs		
A	B	Port 1	Port 2 (Y = A NOR B)	Port 3
0	0	0	1	0
0	1	0	0	1
1	0	1	0	0
1	1	1	0	0

Figure 6.11: Results of NOR Gate using beam propagation method

Impact of Ti strip thickness on IL and ER

In this, impact of Ti strip thickness on power performance of the NOR gate has been investigated by varying the thickness of Ti strip from 0.05 µm to 0.09 µm and plot the graph between the extinction ratio and the thickness of titanium strip and insertion loss and thickness of titanium strip. And we obtain the highest value 29.85 dB of extinction ratio and lowest value of insertion loss 1.103 dB at the 0.05 µm thickness and we increase or decrease the titanium thickness the extinction ratio will be low and insertion ratio will be high.

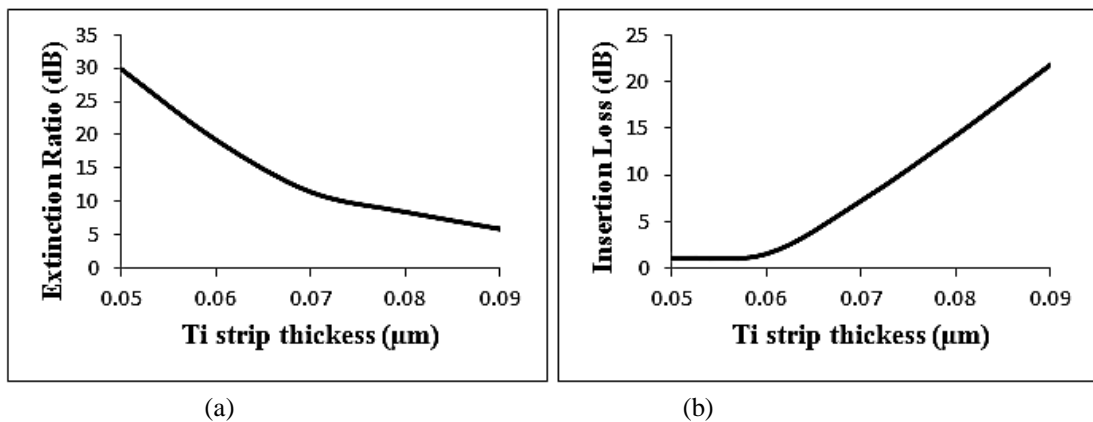(a)   (b)

Figure 6.12: (a) Variation of ER with increase in thickness of Ti strip of NOR Gate (b) Variation of IL with increase in thickness of Ti strip of NOR Gate

6.5 NAND GATE

To implement the NAND gate three MZI's were used, as represented in Fig. 4.9. At the input of MZI-1 and MZI-2 the optical signal is applied and first output port of MZI-3 is taken as output of NAND gate shown in the figure. Fig. 6.13 shows the structure and results of the implemented NAND gate using OptiBPM.

Figure 6.13: Layout structure of NAND Gate

The results of simulation using BPM is shown in Fig. 6.14, where the NAND gate is seen to give acceptable results through proper selection of control signals. The operating principle of the proposed structure can be well monitored using the truth table, Table. 6.5. The results of simulation based analysis have been compared with the BPM results for its validation and verification as shown in Fig. 6.14.

Table 6.5: Inputs and outputs of NAND Gate layout

Control/ Input Signals		Outputs		
A	B	Port 1	Port 2 (Y = A NAND B)	Port 3
0	0	0	1	1
0	1	0	1	0
1	0	1	1	0
1	1	1	0	0
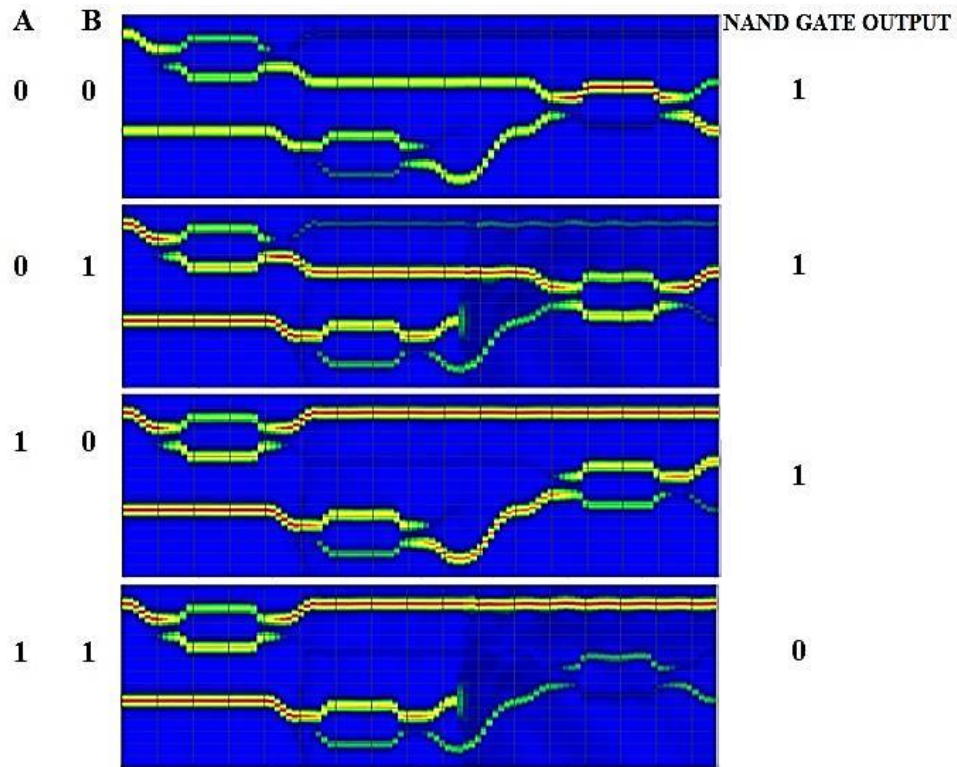
Figure 6.14: Results of NAND Gate using beam propagation method

Impact of Ti strip thickness on IL and ER

In this, impact of Ti strip thickness on power performance of the NAND gate has been investigated by varying the thickness of Ti strip from 0.05 µm to 0.09 µm and plot the graph between the extinction ratio and the thickness of titanium strip and insertion loss and thickness of titanium strip. And we obtain the highest value 17.86 dB of extinction ratio and lowest value of insertion loss 3.182 dB at the 0.05 µm thickness and we increase or decrease the titanium thickness the extinction ratio will be low and insertion ratio will be high.

(a)   (b)

Figure 6.15: (a) Variation of ER with increase in thickness of Ti strip of NAND Gate (b) Variation of IL with increase in thickness of Ti strip of NAND Gate

6.6 XOR GATE

To implement the XOR logic two MZI's were used, as represented in Fig. 4.11. At the input of MZI-1 the optical signal is applied and second output port of MZI-2 is taken as the output XOR operation. Fig. 6.16 shows the structure and results of the XOR gate using OptiBPM.
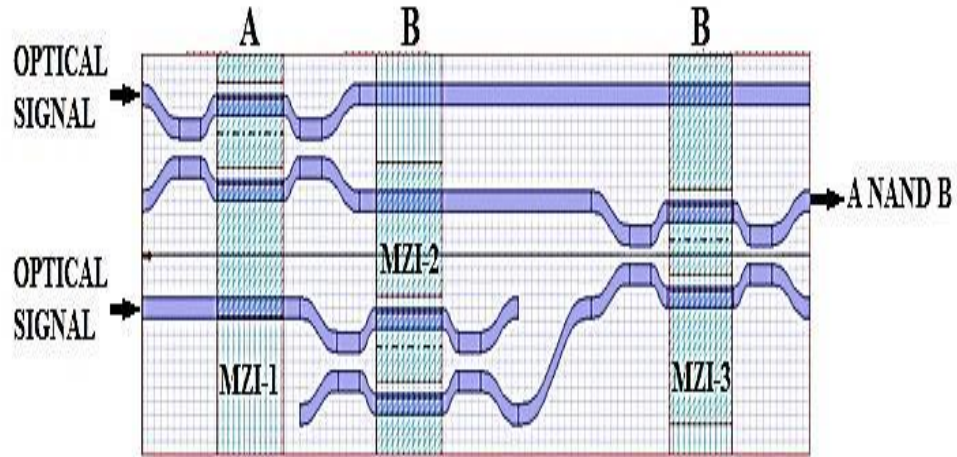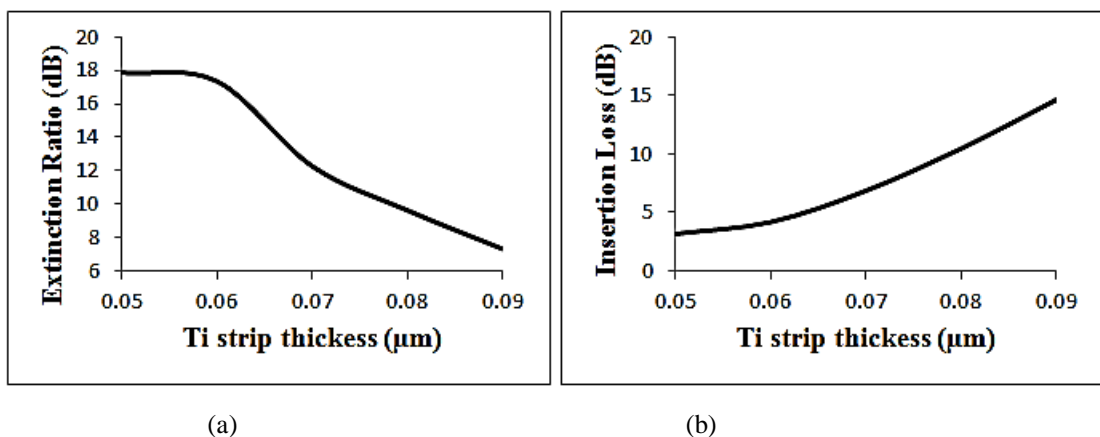

Figure 6.16: Layout structure of XOR Gate

The results of simulation using BPM is shown in Fig. 6.17, where the XOR gate is seen to give acceptable results through proper selection of control signals. The operating principle of the proposed structure can be well monitored using the truth table, Table. 6.6. The results of simulation based analysis has been compared with the BPM results for its validation and verification as shown in Fig. 6.17.

Table 6.6: Inputs and outputs of XOR Gate layout

Control/ Input Signals		Outputs	
A	B	Port 1	Port 2 (C = A XOR B)
0	0	1	0
0	1	0	1
1	0	0	1
1	1	1	0
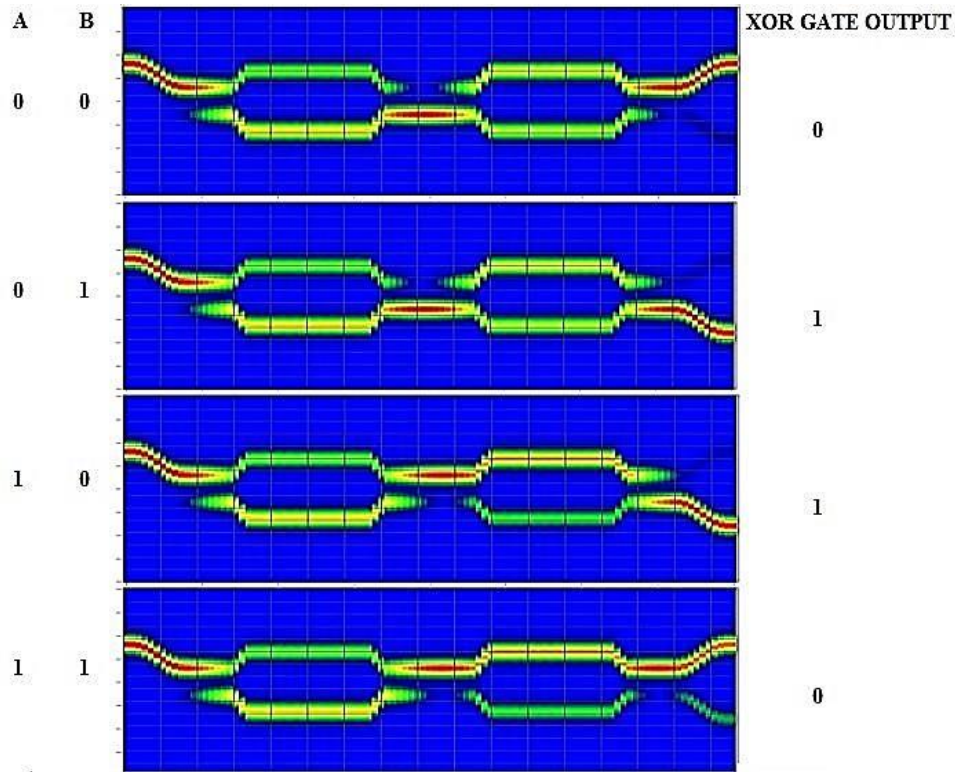
Figure 6.17: Results of XOR Gate using beam propagation method

Impact of Ti strip thickness on IL and ER

In this, impact of Ti strip thickness on power performance of the XOR gate has been investigated by varying the thickness of Ti strip from 0.05 µm to 0.09 µm and plot the graph between the extinction ratio and the thickness of titanium strip and insertion loss and thickness of titanium strip. And we obtain the highest value 13.84 dB of extinction ratio and lowest value of insertion loss 0.128 dB at the 0.05 µm thickness and we increase or decrease the titanium thickness the extinction ratio will be low and insertion ratio will be high.

(a)   (b)

Figure 6.18: (a) Variation of ER with increase in thickness of Ti strip of XOR Gate (b) Variation of IL with increase in thickness of Ti strip of XOR Gate

6.7 XNOR GATE

To implement the XNOR logic two MZI's were used, as represented in Fig. 4.13. At the input of MZI-1 the optical signal is applied and first output port of MZI-2 is taken as the output XNOR operation. Fig. 6.19 shows the structure and results of XNOR gate using OptiBPM.
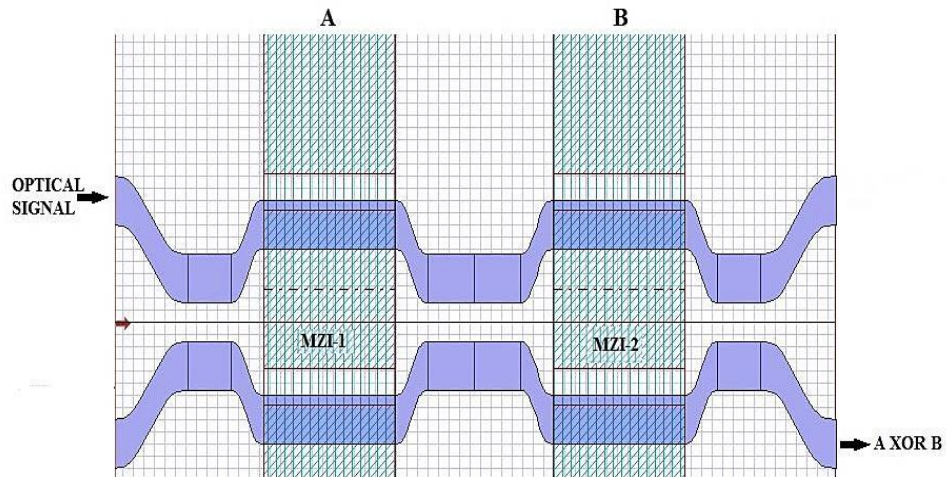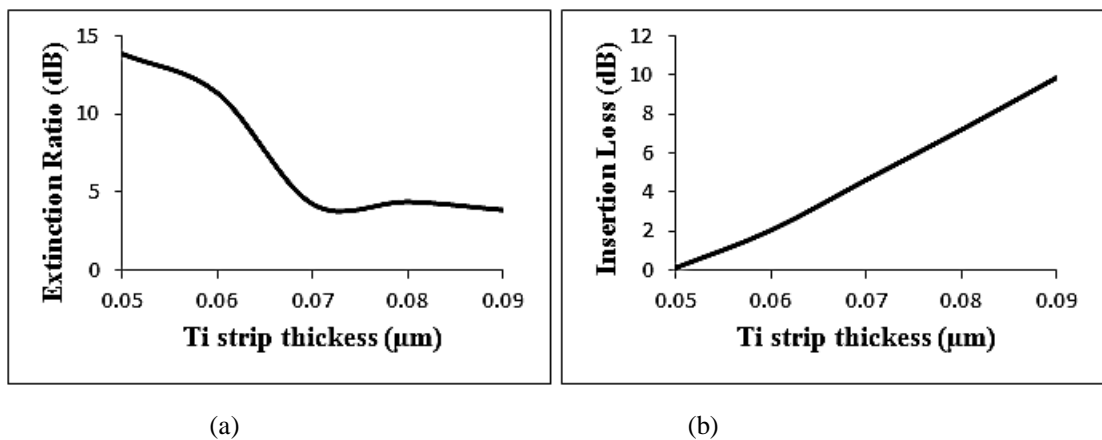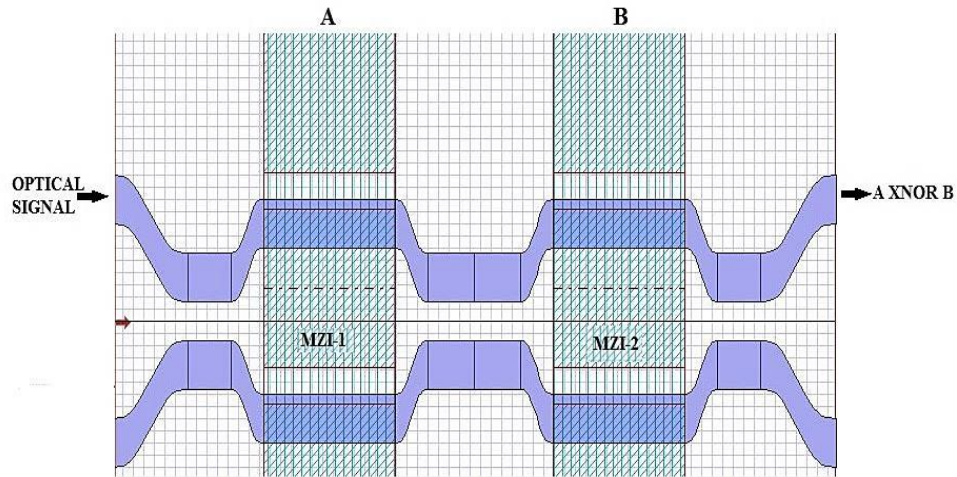

Figure 6.19: Layout structure of XNOR Gate

The results of simulation using BPM is shown in Fig. 6.20, where the XNOR gate is seen to give acceptable results through proper selection of control signals. The operating principle of the proposed structure can be well monitored using the truth table, Table. 6.7. The results of simulation based analysis have been compared with the BPM results for its validation and verification as shown in Fig. 6.20.

Table 6.7: Inputs and outputs of XNOR Gate layout

Control/ Input Signals		Outputs	
A	B	Port 1 (C = A XNOR B)	Port 2
0	0	1	0
0	1	0	1
1	0	0	1
1	1	1	0
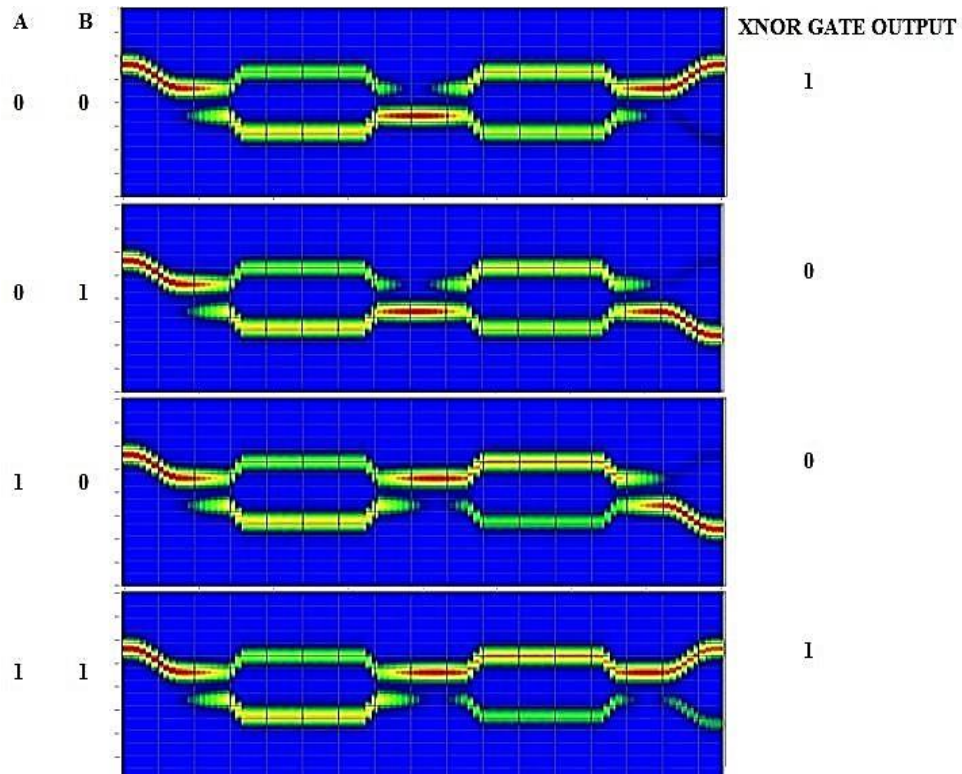
Figure 6.20: Results of XNOR Gate using beam propagation method

Impact of Ti strip thickness on IL and ER

In this, impact of Ti strip thickness on power performance of the XNOR gate has been investigated by varying the thickness of Ti strip from 0.05 µm to 0.09 µm and plot the graph between the extinction ratio and the thickness of titanium strip and insertion loss and thickness of titanium strip. And we obtain the highest value 16.35 dB of extinction ratio and lowest value of insertion loss 0.215 dB at the 0.05 µm thickness and we increase or decrease the titanium thickness the extinction ratio will be low and insertion ratio will be high.

(a)   (b)
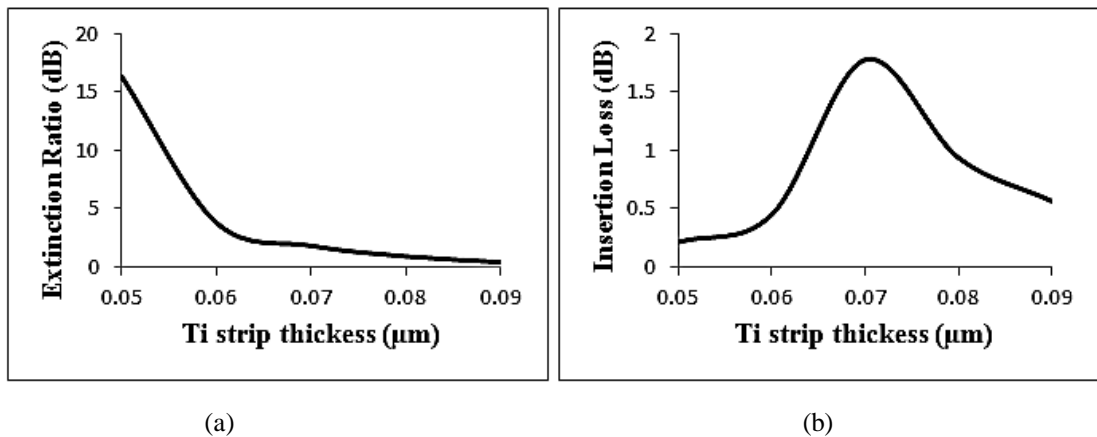
Figure 6.21: (a) Variation of ER with increase in thickness of Ti strip of XNOR Gate (b) Variation of IL with increase in thickness of Ti strip of XNOR Gate

6.8 HALF ADDER

To implement the half adder three MZI's were used, as represented in Fig. 4.15. At the input of MZI-1 the optical signal is applied and second output port of MZI-2 is taken as the output port of the circuit giving the resultant sum of the half adder circuit implemented (XOR operation) and the carry generated by the circuit can be obtained at first output port of MZI-3 as shown in the figure. Fig. 6.22 shows the structure and results of the implemented half adder using OptiBPM.
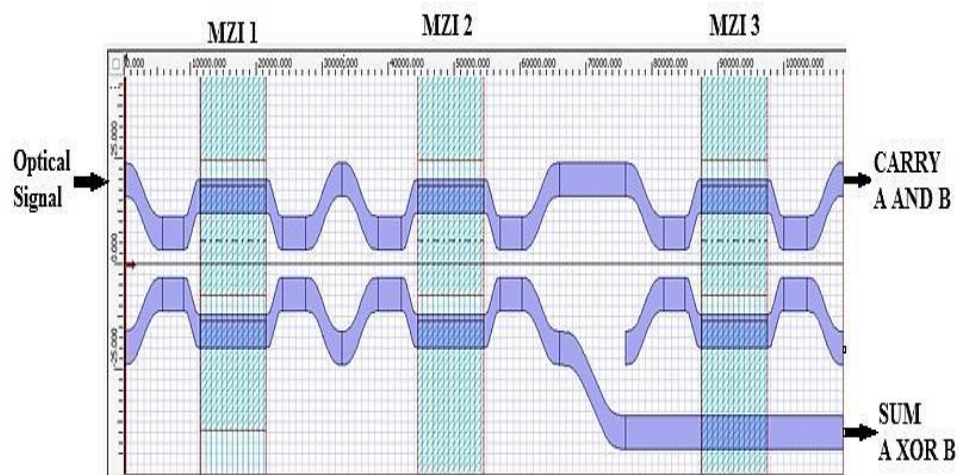
Figure 6.22: Layout structure of Half Adder

The results of simulation using BPM is shown in Fig. 6.23, where the half adder is seen to give acceptable results through proper selection of control signals. The operating principle of the proposed structure can be well monitored using the truth table, Table. 6.8. The results of simulation based analysis have been compared with the BPM results for its validation and verification as shown in Fig. 6.23.

Table 6.8: Inputs and outputs of half adder layout

| Control/ Input Signals		Outputs		
A	B	Port 1 (C = A AND B)	Port 2	Port 3 (S = A XOR B)
0	0	0	1	0
0	1	0	0	1
1	0	0	0	1
1	1	1	0	0
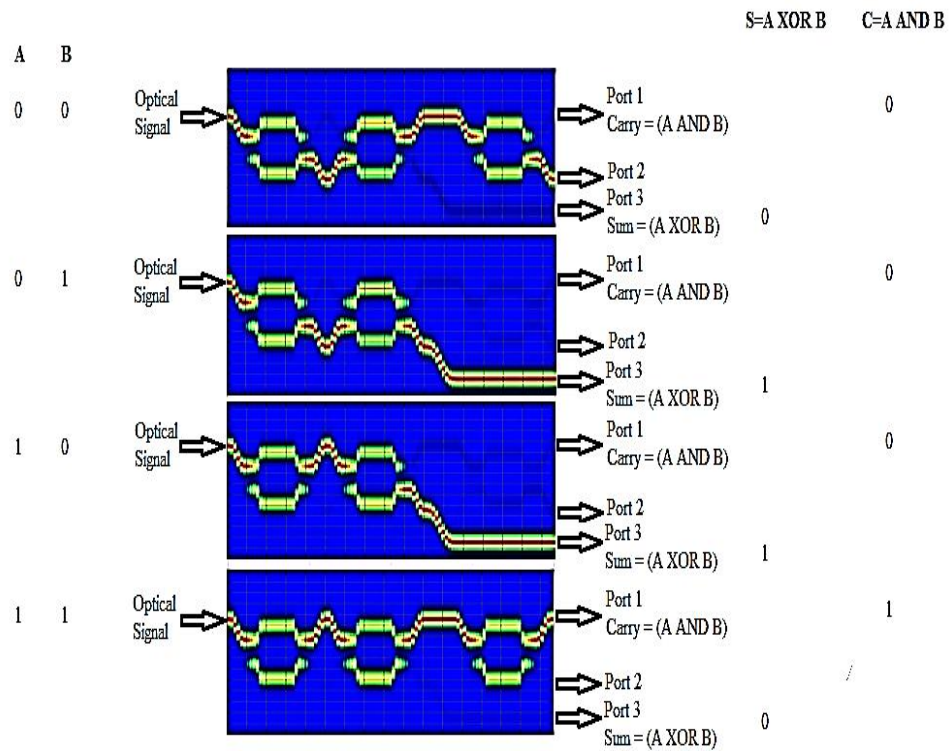
Figure 6.23: Results of half adder using beam propagation method

Impact of Ti strip thickness on IL and ER

In this, impact of Ti strip thickness on power performance of the half adder has been investigated by varying the thickness of Ti strip from 0.05 µm to 0.09 µm and plot the graph between the extinction ratio and the thickness of titanium strip and insertion loss and thickness of titanium strip. And we obtain the highest value 28.68 dB of extinction ratio and lowest value of insertion loss 0.024 dB at the 0.05 µm thickness and we increase or decrease the titanium thickness the extinction ratio will be low and insertion ratio will be high.

(a)   (b)

Figure 6.24: (a) Variation of ER with increase in thickness of Ti strip of half adder (b) Variation of IL with increase in thickness of Ti strip of half adder

CHAPTER 7: CONCLUSION AND FUTURE ASPECTS

7.1 Conclusion

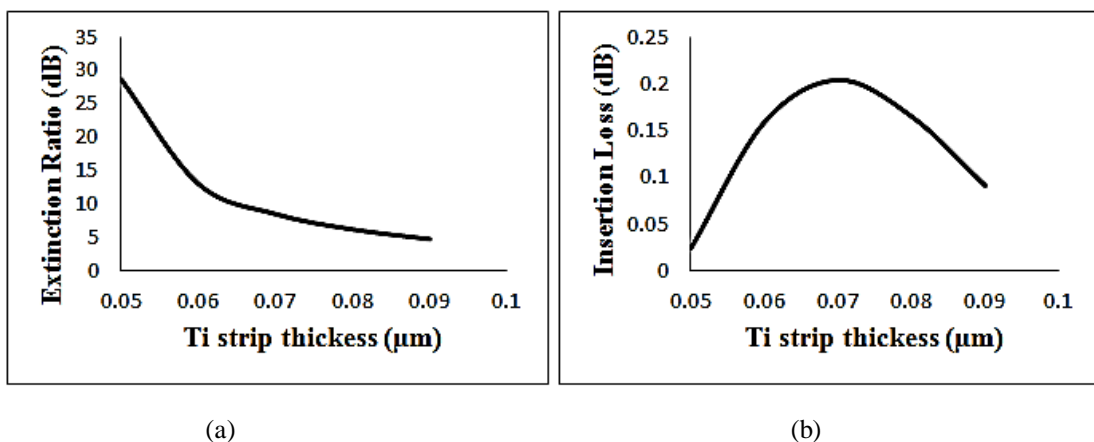In this thesis electro-optic effect has been used in realization of all optical logic gates and half adder circuit using MZIs and beam propagation method has been used for simulation. The advantage of the proposed design is that it requires less number of components than those implemented using SOA-MZI [10]. The results have been compared and verified using MATLAB simulations. The impact of Ti strip thickness variation on the device performance has also been analysed via evaluation of IL and ER. It can be concluded from the analysis that optimum performance of the device can be ensured when Ti strip thickness of 0.05 µm is chosen. The values of ER and IL are obtained theoretically and following values are obtained

- For NOT gate the lowest value of IL obtained in this work is 0.050dB and the maximum value of ER obtained is 26.86 dB.

- For AND gate the lowest value of IL obtained in this work is 0.128dB and the maximum value of ER obtained is 15.13 dB.

- For OR gate the lowest value of IL obtained in this work is 2.531dB and the maximum value of ER obtained is 9.332 dB.

- For NOR gate the lowest value of IL obtained in this work is 1.103dB and the maximum value of ER obtained is 29.85 dB.

- For NAND gate the lowest value of IL obtained in this work is 3.182dB and the maximum value of ER obtained is 17.86 dB.

- For XOR gate the lowest value of IL obtained in this work is 0.128dB and the maximum value of ER obtained is 13.84 dB.

- For XNOR gate the lowest value of IL obtained in this work is 0.215dB and the maximum value of ER obtained is 16.35 dB.

- For Half Adder gate the lowest value of IL obtained in this work is 0.024dB and the maximum value of ER obtained is 26.86 dB.

7.2 Future Aspects

In future, more improvement can be made in the optical logic gates and half adder designs. Future work can be done on following parameters of these modulator designs-

- Size: size can be further reduced for this type of combinational circuit design, compact size devices will result in more small design with lower power consumption.

- Switching Voltage: By reducing the switching voltage more power efficient designs can be made, reduction in switching voltage will result in a decrement of switching voltage length product parameter of MZI structure which is desirable.

- Insertion Loss: lower value of insertion loss for any device is desirable, by working on these designs one can reduce the value of insertion loss more than three digits after decimal point.

- Extinction Ratio: higher value of ER is desirable. So, working on these designs one can increase the value of Extinction Ratio.

- More combinational and sequential circuits can be design using electro optic effect in Mach- Zehnder Interferometer.

BIBLIOGRAPHY

[1] Kumar, Harsh, Laxman Kumar, Vijay Janyani, Buryy Oleh, Ubizskii Serhij, and Ghanshyam Singh. "Gray to binary code converter using Ti-indiffused lithium niobate based Mach-Zehnder interferometer." In Advances in Optical Science and Engineering, pp. 257-262. Springer, Singapore, 2017.

[2] Singh, Ghanshyam, Vijay Janyani, and R. P. Yadav. "Modeling of a high performance Mach--Zehnder interferometer all optical switch." Optica Applicata 42, no. 3 (2012).

[3] Singh, G., V. Janyani, and R. P. Yadav. "Modeling of a 2× 2 electro-optic Mach-Zehnder Interferometer optical switch with s-bend arms." Photonics letters of Poland 3, no. 3 (2011): 119-121.

[4] Kumar, Santosh, Sanjeev Kumar Raghuwanshi, and Ajay Kumar. "Implementation of optical switches using Mach–Zehnder interferometer." Optical Engineering 52, no. 9 (2013): 097106.

[5] Kumar, Ajay, and Sanjeev Kumar Raghuwanshi. "Implementation of optical gray code converter and even parity checker using the electro-optic effect in the Mach–Zehnder interferometer." Optical and Quantum Electronics 47, no. 7 (2015): 2117-2140.

[6] Ganguly, P., D. C. Sen, S. Datt, J. C. Biswas, and S. K. Lahiri. "Simulation of refractive index profiles for titanium indiffused lithium niobate channel waveguides." Fiber & Integrated Optics 15, no. 2 (1996): 135-147.

[7] Kumar, Santosh, Gurdeep Singh, Ashish Bisht, and Angela Amphawan. "Design of D flip-flop and T flip-flop using Mach–Zehnder interferometers for high-speed communication." Applied optics 54, no. 21 (2015): 6397-6405.

[8] Singh, G., R. P. Yadav, and V. Janyani. "Ti indiffused lithium niobate (Ti: LiNbO3) Mach-Zehnder interferometer all optical switches: a review." In New Advanced Technologies. IntechOpen, 2010.

[9] Bremer, T., P. Hertel, S. Oelschig, R. Sommerfeldt, and W. Heiland. "Depth profiling of magnesium-and titanium-doped LiNbO3 waveguides." Thin Solid Films 175 (1989): 235-239.

[10] Kumar, Ajay, Santosh Kumar, and Sanjeev Kumar Raghuwanshi. "Implementation of full-adder and full-subtractor based on electro-optic effect

in Mach–Zehnder interferometers." Optics Communications 324 (2014): 93-107.

[11] Kumar, Santosh, Gurdeep Singh, Ashish Bisht, Sandeep Sharma, and Angela Amphawan. "Proposed new approach to the design of universal logic gates using the electro-optic effect in Mach–Zehnder interferometers." Applied optics 54, no. 28 (2015): 8479-8484.

[12] Kumar, Ajay, Santosh Kumar, and Sanjeev Kumar Raghuwanshi. "Implementation of XOR/XNOR and AND logic gates by using Mach–Zehnder interferometers." Optik-International Journal for Light and Electron Optics 125, no. 19 (2014): 5764-5767.

[13] Kumar, Santosh, and Sanjeev Kumar Raghuwanshi. "Design of optical reversible logic gates using electro-optic effect of lithium niobate based Mach–Zehnder interferometers." Applied optics 55, no. 21 (2016): 5693-5701.

[14] Kumar, Santosh, Ashish Bisht, Gurdeep Singh, Kuldeep Choudhary, K. K. Raina, and Angela Amphawan. "Design of 1-bit and 2-bit magnitude comparators using electro-optic effect in Mach–Zehnder interferometers." Optics Communications 357 (2015): 127-147.

[15] Raghuwanshi, Sanjeev Kumar, Ajay Kumar, and Azizur Rahman. "Implementation of high speed optical universal logic gates using the electro-optic effect-based Mach–Zehnder interferometer structures." Journal of Modern Optics 62, no. 12 (2015): 978-988.

[16] Mohammed, Nazmi A., Huda S. Abo Elnasr, and Moustafa H. Aly. "Performance Evaluation and Enhancement of 2× 2 Ti: LiNbO3 Mach Zehnder Interferometer Switch at 1.3 μm and 1.55 μm." The Open Electrical & Electronic Engineering Journal 6, no. 1 (2012).

[17] Zetie, K. P., S. F. Adams, and R. M. Tocknell. "How does a Mach-Zehnder interferometer work?." Physics Education 35, no. 1 (2000): 46.

[18] Rendón-Salgado, I., and R. Gutiérrez-Castrejón. "160 Gb/s all-optical AND gate using bulk SOA turbo–switched Mach–Zehnder interferometer." Optics Communications 399 (2017): 77-86.

[19] Khatun, Rabeya, Kazi Tanvir Ahmmed, A. Zahed Chowdhury, and Raqibul Hossen. "Optimization of 2× 2 MZI electro-optic switch and its application as logic gate." In 2015 18th International Conference on Computer and Information Technology (ICCIT), pp. 294-299. IEEE, 2015.

[20] Kumar, Santosh, Ajay Kumar, and Sanjeev Kumar Raghuwanshi. "Implementation of an optical AND gate using Mach-Zehnder interferometers." In Optical Modelling and Design III, vol. 9131, p. 913120. International Society for Optics and Photonics, 2014.

[21] Choudhary, Kuldeep, and Santosh Kumar. "Design of pseudorandom binary sequence generator using lithium-niobate-based Mach–Zehnder interferometers." Optical Engineering 56, no. 5 (2017): 057104.

[22] Arvidsson, Gunnar, Kurt Bergvall, and Anders Sjöberg. "Processing of titanium-diffused lithium niobate waveguide devices and waveguide characterization." Thin Solid Films126, no. 3-4 (1985): 177-184.

[23] MS Windows NT introduction of bpm. https://optiwave.com/optibpm-manuals/bpm-introduction-to-optibpm/. Accessed: 2019-06-04.

[24] MS Windows NT mzi switch optiwave. https://optiwave.com/category/optibpm -manuals/optibpm-tutorials/p-lesson-14-mach-zehnder-interferometer-switch/. Accessed: 2019-06-03.

LIST OF PUBLICATION

1. Manisha Prajapat, Ankur Saharia and Ghanshyam Singh, "Design of Half Adder using Electro-Optic Effect in Mach-Zehnder Interferometer" International Conference on Optical and Wireless Technologies (OWT 2019), Springer, Jaipur, India, March 2019.

2. Avneesh , Manisha Prajapat, Ramgopal Ramineni and Rahul, "Study, Design and Evaluation of performance parameters of Optical Logic Gate (NOR)" IETE conference on Advances in Electronic Circuit and Systems, SKIT, Jaipur, April 2018.

Thesis

12% SIMILARITY INDEX   **3**% INTERNET SOURCES   **11**% PUBLICATIONS   **3**% STUDENT PAPERS

1 Santosh Kumar, Gurdeep Singh, Ashish Bisht, Sandeep Sharma, Angela Amphawan. "Proposed new approach to the design of universal logic gates using the electro-optic effect in Mach–Zehnder interferometers", Applied Optics, 2015
Publication

2%

2 Santosh Kumar, Sanjeev Kumar Raghuwanshi, B. M. A. Rahman. "Design of universal shift register based on electro-optic effect of LiNbO3 in Mach–Zehnder interferometer for high speed communication", Optical and Quantum Electronics, 2015
Publication

1%

3 Vijay Sivan, Arnan Mitchell, Lam Bui, Anthony Holland, Suresh Bhargava, Timothy Priest. "Etching of lithium niobate using standard Ti indiffusion technique", Applied Physics Letters, 2007
Publication

1%

Robert J. Simpson, Trevor J. Terrell. "Digital